Experimental and theoretical studies of nanoparticles of antiferromagnetic materials

2007 J. Phys.: Condens. Matter 19 213202

(http://iopscience.iop.org/0953-8984/19/21/213202)

IOP PUBLISHING JOURNAL OF PHYSICS: CONDENSED MATTER

J. Phys.: Condens. Matter **19** (2007) 213202 (31pp) doi:10.1088/0953-8984/19/21/213202

TOPICAL REVIEW

Experimental and theoretical studies of nanoparticles of antiferromagnetic materials

Steen Mørup[1], Daniel E Madsen[1], Cathrine Frandsen[1], Christian R H Bahl[2] and Mikkel F Hansen[3]

[1] Department of Physics, Building 307, Technical University of Denmark, DK-2800 Kgs. Lyngby, Denmark
[2] Fuel Cells and Solid State Chemistry Department, Building 227, Risø National Laboratory, DK-4000 Roskilde, Denmark
[3] MIC—Department of Micro and Nanotechnology, Building 345 East, Technical University of Denmark, DK-2800 Kgs. Lyngby, Denmark

Received 23 January 2007, in final form 13 March 2007
Published 2 May 2007
Online at stacks.iop.org/JPhysCM/19/213202

Abstract

The magnetic properties of nanoparticles of antiferromagnetic materials are reviewed. The magnetic structure is often similar to the bulk structure, but there are several examples of size-dependent magnetic structures. Owing to the small magnetic moments of antiferromagnetic nanoparticles, the commonly used analysis of magnetization curves above the superparamagnetic blocking temperature may give erroneous results, because the distribution in magnetic moments and the magnetic anisotropy are not taken into account. We discuss how the magnetic dynamics can be studied by use of magnetization measurements, Mössbauer spectroscopy and neutron scattering. Below the blocking temperature, the magnetic dynamics in nanoparticles is dominated by thermal excitations of the uniform mode. In antiferromagnetic nanoparticles, the frequency of this mode is much higher than in ferromagnetic and ferrimagnetic nanoparticles, but it depends crucially on the size of the uncompensated moment. Excitation of the uniform mode results in a so-called thermoinduced moment, because the two sublattices are not strictly antiparallel when this mode is excited. The magnetic dipole interaction between antiferromagnetic nanoparticles is usually negligible, and therefore such particles present a unique possibility to study exchange interactions between magnetic particles. The interactions can have a significant influence on both the magnetic dynamics and the magnetic structure. Nanoparticles can be attached with a common crystallographic orientation such that both the crystallographic and the magnetic order continue across the interfaces.

Contents

1. Introduction

Nanoparticles of magnetic materials have attracted much attention because their properties in several ways differ from those of the corresponding bulk materials [1–4]. Therefore, they provide opportunities to make materials and devices with new magnetic properties. Magnetic nanoparticles have numerous technological applications, one of the most important being for data storage in, for example, hard disks in computers [5]. Applications related to medicine and biotechnology are becoming increasingly important [6, 7]. Stable colloidal suspensions of magnetic nanoparticles—so-called ferrofluids—have numerous applications [8], e.g. in loudspeakers. In most applications, ferromagnetic or ferrimagnetic particles are used, because they possess large magnetic moments, and many experimental and theoretical investigations have focused on these types of particles. Nanostructured antiferromagnetic materials have important applications in, for example, spin valves [9, 10] and in the new technology of magnetic random access memory (MRAM) [11]. It has been proposed that nanostructured antiferromagnetic materials may be used to stabilize the magnetization direction of ferromagnetic particles in magnetic recording media [12]. Nanoparticles of antiferromagnetic materials may have interesting applications in, for example, new types of hard magnetic materials consisting of composites of antiferromagnetic and ferromagnetic or ferrimagnetic nanoparticles [13–16].

It is a general feature of magnetic nanoparticles that the (sublattice) magnetization directions may fluctuate because the anisotropy energy may be comparable to the thermal energy. The magnetic anisotropy of nanoparticles is usually assumed to be uniaxial, with the anisotropy energy given by

$$E(\theta) = KV \sin^2 \theta, \tag{1}$$

where K is the magnetic anisotropy energy constant, V is the particle volume and θ is the angle between the (sublattice) magnetization direction and an easy direction of magnetization. Thus, for a nanoparticle with magnetic anisotropy energy given by equation (1), there are minima at $\theta = 0$ and π, separated by an energy barrier, KV. The superparamagnetic relaxation time, i.e., the average time between thermally induced reversals of the (sublattice) magnetization, is approximately given by the Néel–Brown expression [17, 18],

$$\tau = \tau_0 \exp\left(\frac{KV}{k_B T}\right), \tag{2}$$

where k_B is Boltzmann's constant and T is the temperature. The value of τ_0 is typically in the range 10^{-13}–10^{-9} s. The dependence of τ_0 on temperature, particle size, magnetic anisotropy, etc in ferromagnetic nanoparticles has been the subject of several investigations [1]. The superparamagnetic blocking temperature, T_B, is defined as the temperature at which the relaxation time is equal to the timescale of the experimental technique used for studies of the magnetic properties. Thus, the blocking temperature is different for different experimental techniques. In DC magnetization measurements, the timescale is typically of the order of 10 s. Above the blocking temperature, the measured magnetization is the thermal equilibrium value and therefore the coercivity vanishes. Below T_B, the coercivity increases with decreasing temperature. Often, the so-called zero-field-cooled (ZFC) and the field-cooled (FC) magnetization curves are measured after cooling the sample in zero field or in a (small) applied field, respectively, followed by measuring the magnetization as a function of temperature during warming up in the (small) applied field. In the ZFC magnetization curves of magnetic nanoparticles, one can observe a peak at a temperature of the same order of magnitude as the blocking temperature. AC magnetization measurements have the advantage compared to many other techniques that the timescale can be varied by varying the frequency. In Mössbauer spectroscopy, the timescale τ_M is of the order of the nuclear Larmor precession time, i.e., typically a few nanoseconds. Below T_B, the Mössbauer spectra are magnetically split and in the case of ^{57}Fe Mössbauer spectroscopy they consist of a six-line component (a sextet) for each iron site in the material. Above T_B, the spectra consist of singlets or doublets. Because of the distribution of anisotropy energy barriers, KV, the spectra of samples of magnetic nanoparticles normally consist of a superposition of sextets and doublets or singlets in a broad temperature range.

Below the blocking temperature, the thermal energy is insufficient to give rise to frequent magnetization reversals within a time corresponding to the timescale of the experimental technique. However, the (sublattice) magnetization direction may still fluctuate in directions close to an easy direction of magnetization. These fluctuations, termed collective magnetic excitations, can be described as a uniform precession of the (sublattice) magnetization direction around an easy direction in combination with transitions between precession states with different precession angles [19].

It is noteworthy that the uniform precession mode, which can be considered as a spin wave with wavevector $q = 0$, is predominant compared to the spin waves with $q \neq 0$ because of the energy gaps in the spin wave spectrum of nanoparticles [19]. In Mössbauer spectroscopy, the precession and the transitions between the precession states can be considered fast compared to the experimental timescale, and one therefore observes an average value of the magnetic hyperfine field, which for a particle with magnetic energy given by equation (1) can be written at low temperatures [20]:

$$B_{obs} \approx B_0\left[1 - \frac{k_B T}{2KV}\right]. \tag{3}$$

Here B_0 is the saturation hyperfine field. Expressions for the magnetic hyperfine splitting in Mössbauer spectra of nanoparticles with arbitrary form of the anisotropy have also been derived [21], and it has been found as a general rule that collective magnetic excitations give rise to a linear temperature dependence of the (sublattice) magnetization in nanoparticles. This is in contrast to the temperature dependence at low temperatures in bulk materials for which the decrease in (sublattice) magnetization with increasing temperature is predominantly due to spin waves with $q > 0$ and is proportional to T^α, with $\alpha = 3/2$ in ferromagnetic and ferrimagnetic materials and $\alpha = 2$ in antiferromagnetic materials [22]. According to equation (3), measurements of the temperature dependence of the magnetic hyperfine splitting

can be used to estimate the anisotropy constant. There are several contributions to the anisotropy, such as magnetocrystalline anisotropy, shape anisotropy and stress anisotropy. In nanoparticles, the low symmetry around surface ions can also result in a large surface anisotropy [23], and the effective magnetic anisotropy constant is expected to increase with decreasing particle size because of the increase of the relative number of surface atoms.

The timescale in inelastic neutron scattering experiments is much shorter than that of Mössbauer spectroscopy, and this technique can be used to measure the transition energy for transitions between neighbouring uniform precession states [24, 25].

As discussed in sections 3 and 4.4, nanoparticles of antiferromagnetic materials have non-zero magnetic moments and are therefore, strictly speaking, not antiferromagnetic. Anyway, we will for simplicity here use the term 'antiferromagnetic nanoparticles' instead of the more correct term 'nanoparticles of antiferromagnetic materials'. Furthermore, to ease the language we will refer to B $(= \mu_0 H)$ as the magnetic field (in vacuum) as is common in the literature, instead of using the more correct term 'magnetic induction'.

The size dependence of the magnetic properties of antiferromagnetic nanoparticles differs in several ways from that of ferromagnetic and ferrimagnetic nanoparticles [1, 3, 19, 26, 27], and this is one of the reasons for the current interest in antiferromagnetic nanoparticles. In this paper we give a review of the special properties of antiferromagnetic nanoparticles and we will compare with those of ferromagnetic and ferrimagnetic nanoparticles. We emphasize studies of magnetic dynamics and the influence of interparticle interactions on the magnetic properties. In section 2, we give some examples, that illustrate how magnetic structures in antiferromagnetic nanoparticles can deviate from those of the corresponding bulk materials. Although an ideal antiferromagnetic crystal has no net magnetic moment, nanoparticles of antiferromagnetic particles usually have non-zero magnetic moments, and this is discussed in section 3. Section 4 deals with fluctuations of the sublattice magnetization direction in antiferromagnetic nanoparticles, and it is discussed how such fluctuations can be studied by different experimental techniques, such as magnetization measurements, Mössbauer spectroscopy and neutron scattering. We discuss the special features of the uniform mode in antiferromagnetic nanoparticles, and furthermore, the existence of thermoinduced magnetization and macroscopic quantum tunnelling phenomena are discussed. In section 5 we give a short review of studies of the influence of magnetic interactions between antiferromagnetic nanoparticles.

2. Magnetic structure of antiferromagnetic nanoparticles

The magnetic structure of nanoparticles may for several reasons differ from that of the corresponding bulk materials. By use of ^{57}Fe Mössbauer spectroscopy, one can often get information about magnetic structures by measuring the relative areas of the six absorption lines. In the case of nanoparticles of ferrimagnetic materials, several ^{57}Fe Mössbauer studies have shown that the intensity of lines 2 and 5 does not vanish when large magnetic fields are applied parallel to the gamma-ray direction, as expected for a perfect ferrimagnet for which the sublattice magnetization directions should be parallel or antiparallel to the applied field [28–30]. This suggests that the reduced number of magnetic neighbour ions at the surface may give rise to magnetic frustration and a related localized spin-canting. It has been suggested [29] that ferrimagnetic nanoparticles can be described as consisting of a magnetically ordered core and a disordered (canted) shell with a thickness of the order of 1–2 nm. However, this model may be too simple in most cases, because defects in the interior of the particles also can result in spin-canting [31]. It is likely that spin-canting is also present in nanoparticles of antiferromagnetic materials [26]. In a recent Mössbauer study of nanoparticles of antiferromagnetic ^{57}Fe-doped NiO [32], a strong indication of spin-canting was observed.

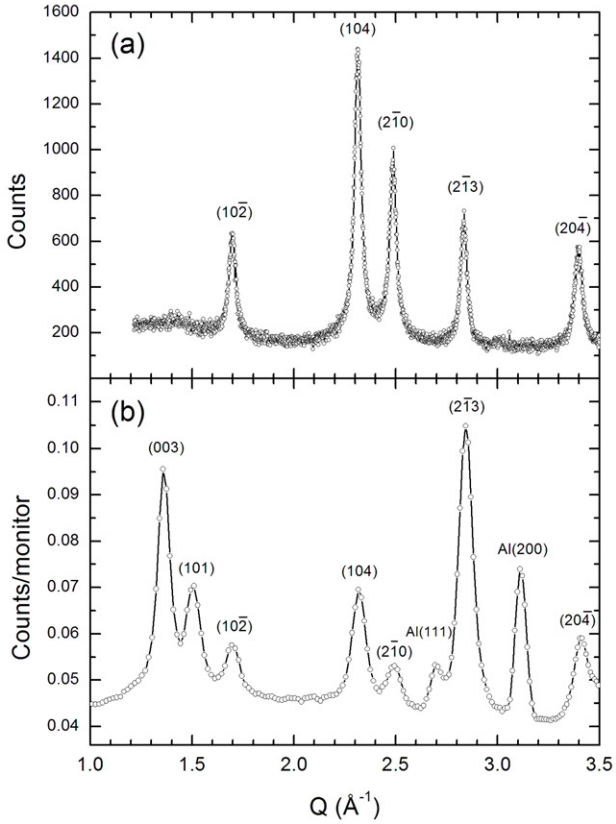

Figure 1. (a) X-ray diffraction data and (b) neutron diffraction data for 15 nm hematite nanoparticles. Reprinted with permission from [35]. Copyright 2000 by the American Physical Society.

Theoretical studies of NiO nanoparticles [33, 34] have shown that the interior magnetic structure can differ from the bulk magnetic structure, because of the influence of surface effects. NiO nanoparticles may have a complex magnetic structure with as many as eight sublattices [33], in contrast to bulk NiO, which has a simple two-sublattice structure.

Neutron diffraction allows for resolving magnetic structures of crystals. Figure 1(b) shows room-temperature neutron powder diffraction data of 15 nm α-Fe_2O_3 particles [35]. For comparison, x-ray powder diffraction data for the same particles are displayed in figure 1(a). The neutron data show the hexagonal (003) and (101) diffraction peaks at the scattering vectors $Q = 1.37$ and 1.50 Å^{-1}, respectively. These peaks are not present in the x-ray data as they are purely magnetic. The magnetic diffraction data are in accordance with the magnetic structure of bulk α-Fe_2O_3 at the same temperature. The magnetic correlation length can be estimated from the width of these diffraction lines using the Scherrer formula in the same way as the crystallographic correlation length can be estimated from the width of the x-ray diffraction lines. The analysis of the data in figure 1 showed that the magnetic and the crystallographic correlation length are identical, i.e., each particle seems to consist of a single magnetic domain [35]. Similar results were found in neutron diffraction studies of NiO [36]. MnO nanoparticles also have the same magnetic structure as the bulk material, but the magnetic correlation length was reported to be smaller than the crystallographic correlation length [37].

Cr nanoparticles have been found to have a simple antiferromagnetic structure, which differs from the spin-density wave structure of bulk Cr [38].

The reduced number of magnetic neighbour ions at the surface results in a smaller exchange field at the surface than in the interior of particles. As a consequence, the (sublattice) magnetization near the surface decreases more quickly with temperature than the (sublattice) magnetization in bulk materials. This has been illustrated by Mössbauer spectroscopy studies of particles of α-Fe_2O_3, which were prepared with a core with only ^{56}Fe and a thin surface layer with ^{57}Fe, such that only the surface atoms contribute to the spectra [39]. Similar results have been found for β-FeOOH [40] and α-FeOOH [41]. The experimental results show an almost linear temperature dependence of the surface magnetization, which is qualitatively in accordance with theoretical models [26, 36, 39, 42]. The temperature dependence of the surface magnetization of these antiferromagnetic nanoparticles is similar to that of ferrimagnetic γ-Fe_2O_3 (maghemite) nanoparticles [39].

When determining the Néel temperature of antiferromagnetic nanoparticles, it is important to be able to distinguish between a transition from a blocked to a superparamagnetic state and a transition to a paramagnetic state. This is not always straightforward, and therefore a careful data analysis may be needed in studies of the size dependence of the Néel temperature. Neutron diffraction studies of plate-shaped, NiO nanoparticles with a thickness of only 2 nm indicated a reduction of the Néel temperature by around 60 K [36]. This is in accordance with theoretical estimates, which showed a lowering of the Néel temperature that depends crucially on the thickness of the NiO plates. Similar neutron studies of much bigger α-FeOOH nanoparticles (particle length $\sim$50 nm and width $\sim$12 nm) [43] also suggested a significant lowering of the Néel temperature (by about 40 K). Both magnetization [44] and μSR [45] measurements of CuO nanoparticles seem to indicate a decreasing Néel temperature with decreasing particle size. In a neutron diffraction study of MnO particles with dimensions of about 14 nm in a porous silica matrix, a slight increase of the Néel temperature has been reported [37]. It was suggested that this could be explained by interaction with the support.

Another type of size dependence of the magnetic structure has been reported in antiferromagnetic α-Fe_2O_3 (hematite) nanoparticles. In bulk α-Fe_2O_3, the sublattice magnetization directions are parallel to the hexagonal [001] direction below the so-called Morin temperature, $T_M \approx 263$ K. The Morin transition takes place because of a change of the sign of the magnetic anisotropy constant. Above this temperature, the sublattice magnetization directions lie in the (001) plane, and the two sublattices are not strictly antiparallel, but form an angle of about 0.15°, which results in a small net magnetization. In nanoparticles it has been found that the Morin transition temperature decreases with decreasing particle size [46–48], and it has been reported to be absent for particles with diameters below around 20 nm. This size dependence of the Morin transition temperature can be explained by a size dependence of the magnetic anisotropy constants [49].

Antiferromagnetic materials may perform a so-called spin–flop transition in large applied magnetic fields, such that the sublattice magnetization vectors become nearly perpendicular to the applied magnetic field. If the magnetic field is applied along the easy axis of a simple two-sublattice uniaxial antiferromagnet, the spin–flop transition field at low temperatures is given by [22]

$$B_{sf} \approx \sqrt{2B_E B_A}, \tag{4}$$

where B_E is the exchange field and $B_A = K/M_S$ is the anisotropy field of an antiferromagnet with sublattice magnetization M_S. It is here assumed that $B_E \gg B_A$. If an uncompensated moment (see section 3) is present, the spin–flop transition field will be enhanced [50]. In a study of the spin–flop transition in samples of α-Fe_2O_3 nanoparticles with average size in

the range from 36 to 159 nm, it was found that the critical field for the spin–flop transition decreases with decreasing particle size [51]. These particles are so large that the influence of an uncompensated magnetic moment may be insignificant. It was suggested that the size dependence of the spin–flop transition field may be explained by a decrease of the exchange field with decreasing particle size due to surface effects.

Ferritin is an iron storage protein with an antiferromagnetic iron-containing core. In a recent study of ferritin particles with a magnetic core size of about 7 nm, no spin–flop transition was found even in applied fields up to 55 T [52], although B_{sf} of ferritin according to equation (4) should be less than 10 T [53]. This result may be explained by the large uncompensated magnetic moment in these particles (see section 3) [50].

3. The magnetic moment of antiferromagnetic nanoparticles

Numerous magnetization studies of antiferromagnetic nanoparticles have shown that both the initial susceptibility and the magnetization in large applied fields are considerably larger than in the corresponding bulk materials. It was suggested by Néel [54] that this may be due to the finite number of magnetic atoms in nanoparticles, which may lead to a difference in the numbers of spins in the two sublattices because of random occupancy of lattice sites. This results in an uncompensated magnetic moment, μ_u. In one specific model, Néel considered nanoparticles with a random occupancy of all the lattice sites and found that the number of uncompensated spins should be of the order of $N^{1/2}$, where N is the total number of spins in a particle. If the interior of the particles is assumed defect-free, but there is a random occupancy of surface sites, the number of uncompensated spins should instead be proportional to the square root of the number of surface sites, i.e., proportional to $N^{1/3}$. In a third model, Néel considered particles consisting of either an even or an odd number of planes with parallel spins, but with alternating magnetization directions. In this case, the number of uncompensated spins should rather be proportional to $N^{2/3}$.

In experimental studies of the magnetization of antiferromagnetic nanoparticles, the presence of impurities can be crucial [55]. Even tiny amounts of strongly magnetic phases, which may not be visible in x-ray diffraction measurements, may dominate the magnetization of the samples. During the preparation of many antiferromagnetic nanoparticles, impurity phases can be difficult to avoid. For example, when preparing CoO nanoparticles, the samples may be contaminated with ferromagnetic metallic Co or antiferromagnetic Co_3O_4 with a lower Néel temperature. Similarly, CuO nanoparticles may be contaminated with Cu_2O, which seems to become increasingly stable with decreasing particle size [56]. In samples of α-Fe_2O_3 nanoparticles, a few per cent of ferrihydrite, which also is antiferromagnetic, can give a large contribution to the magnetization [35].

Experimental studies of the magnetization of samples of NiO nanoparticles with different average size [55] and without impurities of either ferromagnetic metallic Ni or Ni^{3+} ions have suggested that the size dependence of the magnetic moment was proportional to $N^{1/3}$, i.e., the magnetic moments can be explained by a random occupation of surface sites, and the magnetic moment of a nanoparticle is then approximately proportional to its diameter. Recently, high-field Mössbauer studies of plate-shaped NiO nanoparticles have been used to estimate the magnitude of the uncompensated magnetic moment [32]. The spectra were analysed by use of a model [57], in which the influence of the magnetic anisotropy and the uncompensated magnetic moment on the positions and relative areas of the Mössbauer lines was taken into account. The estimated value of μ_u was also in this case in accordance with a random occupation of surface sites [32].

The magnetic core in ferritin is usually poorly crystalline. For such particles, the uncompensated magnetic moment has been found to be of the order of $N^{1/2}$ [53, 58–60],

suggesting a more or less random occupation of all lattice sites. Ferrihydrite particles, which have a disordered structure similar to that of ferritin cores, also have magnetic moments of the order of $N^{1/2}$ [61].

It has recently been suggested that the magnetic moment of nanoparticles of antiferromagnetic materials has a contribution, μ_t, from so-called thermoinduced magnetization [62]. This contribution is related to the fact that the two sublattices of a simple antiferromagnet are not strictly antiparallel when the uniform mode is excited, and the difference in precession angles increases with increasing temperature, such that the net magnetic moment increases with increasing temperature. This is discussed in more detail in section 4.4. In general, the total magnetic moment of an antiferromagnetic nanoparticle is expected to have contributions from both uncompensated spins and a thermoinduced moment [62, 63].

In many experimental studies of the magnetization of magnetic nanoparticles, the magnetization has been measured as a function of the applied magnetic field, B_{ext}, at different temperatures. Typically, the magnetization curves above the blocking temperature have been fitted with a Langevin function

$$L\left(\frac{\mu B_{ext}}{k_B T}\right) = \coth\left(\frac{\mu B_{ext}}{k_B T}\right) - \frac{k_B T}{\mu B_{ext}}, \tag{5}$$

where μ is the magnetic moment of a particle. This model has been successfully used to fit data for ferromagnetic and ferrimagnetic nanoparticles. In most fits of magnetization data for antiferromagnetic nanoparticles, a linear term was also included to account for the antiferromagnetic susceptibility such that the magnetization curves were fitted to the expression

$$\langle M\rangle_T = M_0(T)L\left(\frac{\mu B_{ext}}{k_B T}\right) + \mu_0^{-1}\chi_{AF}B_{ext}, \tag{6}$$

where M is the magnetization, $M_0(T)$ is the saturation magnetization at temperature T, μ_0 is the vacuum permeability and χ_{AF} is the antiferromagnetic susceptibility. It has been found in many experimental studies of antiferromagnetic nanoparticles that this model gives good fits to the experimental data. In several studies, the estimated magnetic moments were surprisingly found to increase with increasing temperature [58, 59, 61, 64, 65]. This is consistent with a contribution from thermoinduced magnetization [62]. It has, however, been pointed out by Silva *et al* [66] that the distribution of the magnitude of the magnetic moments in a sample also can explain such data. This is because the smallest magnetic moments are far from being saturated at high temperatures and therefore give an almost linear contribution to the magnetization, which may be attributed to the antiferromagnetic susceptibility. Thus, when the temperature is increased, the fitted Langevin functions will be increasingly dominated by the larger magnetic moments, and this may at least partly explain the apparent increase of the magnetic moment.

The magnetic anisotropy is usually neglected in the fits of magnetization curves of nanoparticles, but especially in the case of antiferromagnetic nanoparticles this can result in erroneous results [67]. The Langevin function may be a good approximation to the magnetization above the blocking temperature if the Zeeman energy ($\sim\mu B_{ext}$) is large compared to the anisotropy energy ($\sim KV$). However, even for ferromagnetic and ferrimagnetic nanoparticles with relatively large magnetic moments, a finite magnetic anisotropy can give rise to deviations from the Langevin behaviour [68, 69]. In antiferromagnetic nanoparticles with relatively small magnetic moments, the Zeeman energy will often be small compared to the anisotropy energy, and the deviation of the magnetization curves from the Langevin function may therefore be significant. Figure 2 shows simulated magnetization curves for particles with

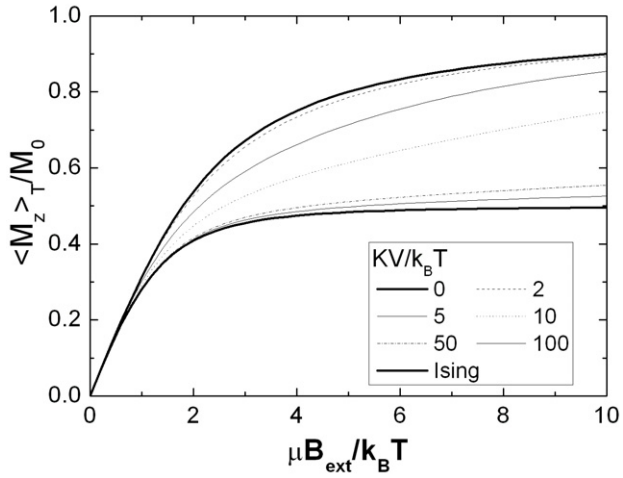

Figure 2. Simulated magnetization curves of antiferromagnetic nanoparticles above the blocking temperature showing the normalized magnetization as a function of $\mu B_{\text{ext}}/k_{\text{B}}T$ for various values of the anisotropy parameter $KV/k_{\text{B}}T$. Reprinted with permission from [67]. Copyright 2006 by Elsevier.

uniaxial anisotropy and a random orientation of the easy axes as a function of $\mu B_{\text{ext}}/k_{\text{B}}T$ for various values of the anisotropy energy parameter $KV/k_{\text{B}}T$. In the simulations, it was assumed that the temperature is above the blocking temperature. No linear terms due to the antiferromagnetic susceptibility were included in these simulations. It is clearly seen that a finite anisotropy changes the shape of the magnetization curves, and especially for values of $KV/k_{\text{B}}T$ of the order of 5–10, the magnetization curves show a slope at high fields, which erroneously might be attributed to an antiferromagnetic susceptibility. For this reason, the parameters obtained from fits of magnetization curves for antiferromagnetic nanoparticles with equation (6) may be incorrect.

Above the blocking temperature, the initial susceptibility of a sample of non-interacting nanoparticles with a finite anisotropy and with a random orientation of easy axes is given by [32, 67, 70]

$$\chi_i = \frac{n\mu_0}{3k_{\text{B}}T}\langle\mu^2\rangle + \chi_{\text{AF}}, \tag{7}$$

where n is the number of particles per volume and χ_{AF} is the antiferromagnetic susceptibility, which may be comparable to the bulk value [55]. It is remarkable that the first term in equation (7) is independent of the anisotropy energy constant. Moreover, it is also independent of the detailed shape of the distribution of the magnetic moments of the particles in the sample. It has therefore been suggested [32, 67] that one should focus on the initial susceptibility in magnetization studies of antiferromagnetic particles.

As will be discussed in section 5, antiferromagnetic nanoparticles may interact strongly via exchange interactions between surface atoms of neighbouring particles. Interparticle interactions can also have a large influence on the magnetic moments that are derived by use of equation (7) [32, 71, 72]. Therefore, equation (7) should only be used to estimate magnetic moments of non-interacting nanoparticles.

Below the blocking temperature, the hysteresis loops of samples of antiferromagnetic nanoparticles show some unusual properties. Studies of, for example, ferritin [60], NiO [33, 73], CuO [44], Co_3O_4 [74], MnO [75] and Cr_2O_3 [65] have shown very large coercivities, and after field cooling antiferromagnetic nanoparticles often show exchange bias.

These features can be explained by the exchange coupling between the uncompensated spins and the antiferromagnetic regions. In the case of NiO nanoparticles it has also been suggested that the phenomena can be explained by a multi-sublattice structure [33, 76].

4. Magnetic fluctuations in non-interacting antiferromagnetic nanoparticles

As discussed in section 1, the magnetization direction in nanoparticles fluctuates at finite temperatures, such that the magnetization directions frequently are reversed in the superparamagnetic region and are affected by collective magnetic excitations at lower temperatures. Here, we give an overview of the application of various experimental techniques for studies of magnetic fluctuations in antiferromagnetic nanoparticles.

4.1. Magnetization measurements

In DC magnetization studies of nanoparticles, the magnetic dynamics are commonly studied by ZFC and FC magnetization measurements. If a sample of non-interacting particles is truly monodisperse, the ZFC magnetization curve will have a maximum at the blocking temperature. However, a sample of ferromagnetic or ferrimagnetic particles with a particle size distribution will have its maximum at a higher temperature, T_{peak} [77, 78], i.e., $T_{\mathrm{peak}} = \beta T_{\mathrm{bm}}$, where $\beta > 1$ and T_{bm} is the median blocking temperature corresponding to the median volume V_{m}, defined such that the sum of the volumes of the particles with $V > V_{\mathrm{m}}$ contributes 50% of the total volume. The value of the parameter β depends on the size distribution. For samples with a log-normal distribution, β increases from 1.0 to around 2.0 when σ_V (the standard deviation of $\ln V$) is increased from 0.0 to 1.5 [79]. In antiferromagnetic nanoparticles with an uncompensated magnetic moment, the magnetic moment is not proportional to the volume as is the case for ferromagnetic particles. Therefore, there may not be a simple relation between the values of β and σ_V. Some experimental studies have suggested that the uncompensated moment may be proportional to the diameter [32, 55]. In this case, the value of the parameter β has been found to decrease with increasing values of σ_V in a log-normal distribution [79].

It is important to realize that the magnetic susceptibility of antiferromagnets has a maximum at the Néel temperature [22]. Therefore, a peak in a ZFC magnetization curve may not always be related to a superparamagnetic blocking temperature, but it may be due to a transition from an antiferromagnetic state to a paramagnetic state.

If the moment distribution is known, the superparamagnetic blocking temperature can be estimated from T_{peak} in a ZFC magnetization curve, but since there usually are two unknown parameters, τ_0 and K, in equation (2), both of these parameters cannot be estimated from a ZFC magnetization curve. However, this is possible by using AC susceptibility measurements with different frequencies. In AC susceptibility measurements one measures the complex susceptibility, which can be written [78]

$$\chi_{\mathrm{AC}}(\omega, T) = \chi'(\omega, T) + \mathrm{i}\chi''(\omega, T), \tag{8}$$

where χ' and χ'' are the in-phase and the out-of-phase components of the measured susceptibility, respectively, and ω is the angular frequency. The in-phase susceptibility has a maximum at a temperature T_{max}, which is related to the blocking temperature and the particle size distribution as for the ZFC magnetization curve. The temperature corresponding to the maximum of the out-of-phase susceptibility is less sensitive to the size distribution and thus an analysis based on just the maxima is better carried out using χ'' data. Such data can, however, be difficult to measure accurately for low-moment samples, and therefore in many studies of antiferromagnetic nanoparticles only χ' data have been reported. Several AC susceptibility

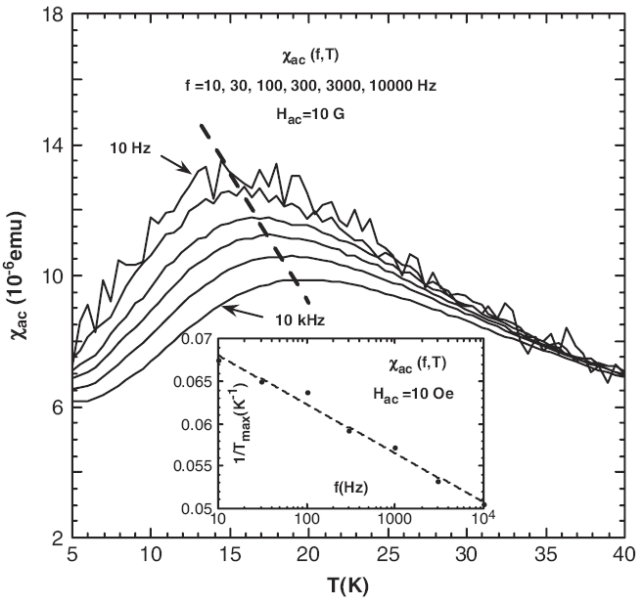

Figure 3. In-phase AC magnetic susceptibility of horse spleen ferritin as a function of temperature at several frequencies, f. The dashed line indicates the peak positions. In the inset is shown $1/T_{\max}$ versus $\log f$. Reprinted with permission from [52]. Copyright 2007 Elsevier.

measurements have been made on ferritin [52, 59, 80, 81] and α-Fe_2O_3 [35]. In studies of superparamagnetic relaxation, ferritin has the advantage that the magnetic cores are well separated by organic non-magnetic material such that the influence of interparticle interaction is negligible. Figure 3 shows in-phase susceptibility data for horse spleen ferritin obtained at frequencies in the range $f = \omega/2\pi = 10$–$10\,000$ Hz [52]. As indicated by the dashed line, the peak position is, as expected, shifted towards higher temperatures, when the frequency is increased. The inset shows that $1/T_{\max}$ varies linearly with $\log f$ in accordance with equation (2). From these data an anisotropy energy constant of $K = 2.5 \times 10^4$ J m^{-3} and a value of τ_0 s $\approx 10^{-12}$–10^{-13} were estimated [52].

4.2. Mössbauer spectroscopy studies

Mössbauer spectroscopy has been extensively used for studies of superparamagnetic relaxation and collective magnetic excitations in nanoparticles. As the timescale of Mössbauer spectroscopy, τ_M, is of the order of a few nanoseconds, it is a good supplement to DC and AC magnetization measurements. By combining ZFC magnetization measurements and Mössbauer data for ferritin, Dickson *et al* [82] estimated a value of τ_0 similar to that obtained by the AC susceptibility measurements discussed above.

The values of τ_0 and K can also be estimated from series of Mössbauer spectra obtained at different temperatures. As an example of such a Mössbauer study of non-interacting antiferromagnetic nanoparticles, figure 4 shows spectra of 15 nm α-Fe_2O_3 particles at different temperatures [35]. The spectra show the typical features of superparamagnetic nanoparticles. At low temperatures, the spectra are magnetically split because the superparamagnetic relaxation is slow compared to τ_M. With increasing temperature, an increasing number of particles have relaxation times shorter than τ_M, resulting in an increasing area of a

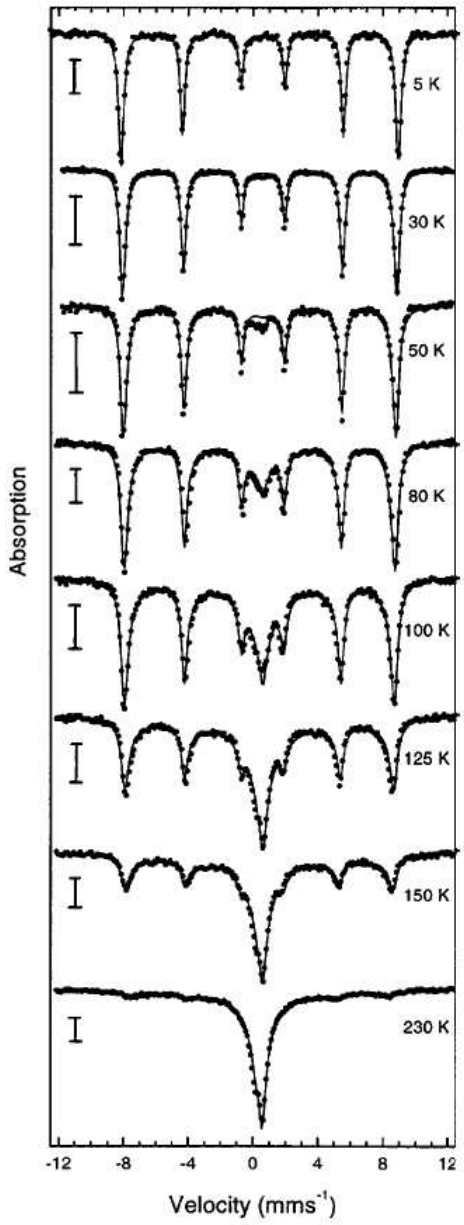

Figure 4. Mössbauer spectra of 15 nm hematite nanoparticles measured at the indicated temperatures. The solid lines are fits obtained as described in the text. Reprinted with permission from [35]. Copyright 2000 by the American Physical Society.

central doublet in the spectra. The fits shown in the figure were obtained using the Blume–Tjon model [83] for Mössbauer relaxation spectra, taking into account the particle size distribution [35]. All the spectra were fitted simultaneously, assuming that the superparamagnetic relaxation time is given by equation (2). From the fits, the values $\tau_0 \approx 5.0 \times 10^{-11}$ s and $KV/k_B \approx 600$ K (corresponding to $K \approx 4500$ J m^{-3}) were estimated [35]. Similar fits of temperature series of Mössbauer spectra of a number of samples of α-Fe_2O_3

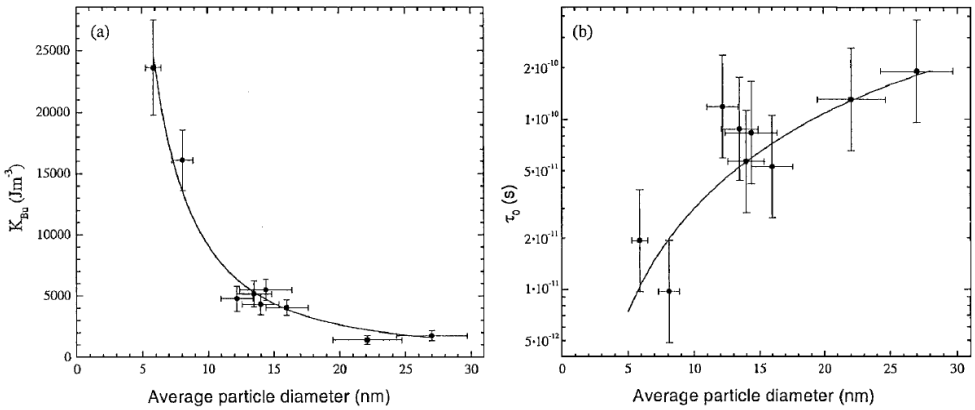

Figure 5. (a) Magnetic anisotropy constant and (b) the prefactor τ_0 for α-Fe_2O_3 nanoparticles as a function of particle diameter. Reprinted with permission from [46].

nanoparticles with average particle diameter in the range $d \approx 6$–30 nm have been used to estimate the size dependence of K and τ_0 [46]. The data are shown in figure 5. It can be seen in figure 5(a) that the magnetic anisotropy constant increases significantly with decreasing particle size, especially for the smallest particles. This is presumably because of the influence of surface anisotropy. Qualitatively similar results for the size dependence of the magnetic anisotropy constants have been found for ferrimagnetic γ-Fe_2O_3 [84] and ferromagnetic α-Fe particles [85]. The data for α-Fe_2O_3 nanoparticles can be fitted well with an empirical d^{-2} dependence of the magnetic anisotropy constant [46, 86]. This implies, according to equation (3), that the reduction of the magnetic hyperfine field at a given temperature should be proportional to d^{-1}. Such a size dependence has also been found for maghemite nanoparticles [84] and in several studies of magnetic nanoparticles in soil samples [86]. The data in figure 5(b) show that the value of τ_0 decreases with decreasing particle size.

Ferromagnetic and ferrimagnetic nanoparticles usually have relatively large magnetic moments, typically in the range 10^3–10^5 Bohr magnetons, and even in relatively small applied fields ($B_{\text{ext}} \lesssim 1$ T) at ambient temperature, the Zeeman energy may be larger than the thermal energy. Consequently, the superparamagnetic relaxation above T_B can be suppressed by relatively small external fields. As discussed in section 3, the Zeeman energy of ferromagnetic and ferrimagnetic nanoparticles in moderate applied fields is typically also larger than the anisotropy energy. The magnetic splitting of the Mössbauer spectra is then to a good approximation proportional to the sum of the external field and a contribution proportional to the Langevin function. At large applied fields ($\mu B_{\text{ext}} \gg k_B T$) the hyperfine splitting can be approximated by the simple expression [87]

$$B_{\text{obs}} = B_0\left(1 - \frac{k_B T}{\mu B_{\text{ext}}}\right) - B_{\text{ext}}. \tag{9}$$

(The minus in front of B_{ext} is due to the fact that the direction of the hyperfine field is usually opposite to that of the applied field.) Thus a plot of $B_{\text{obs}} + B_{\text{ext}}$ as a function of B_{ext}^{-1} gives a straight line with a slope from which the magnetic moment can be estimated.

In antiferromagnetic nanoparticles which have smaller magnetic moments (typically of the order of a few hundred Bohr magnetons), much larger fields are required to suppress the superparamagnetic relaxation to the same extent. Figure 6 shows Mössbauer spectra of human spleen ferritin at 100 K in applied magnetic fields up to 10 T [88]. The zero-field spectrum

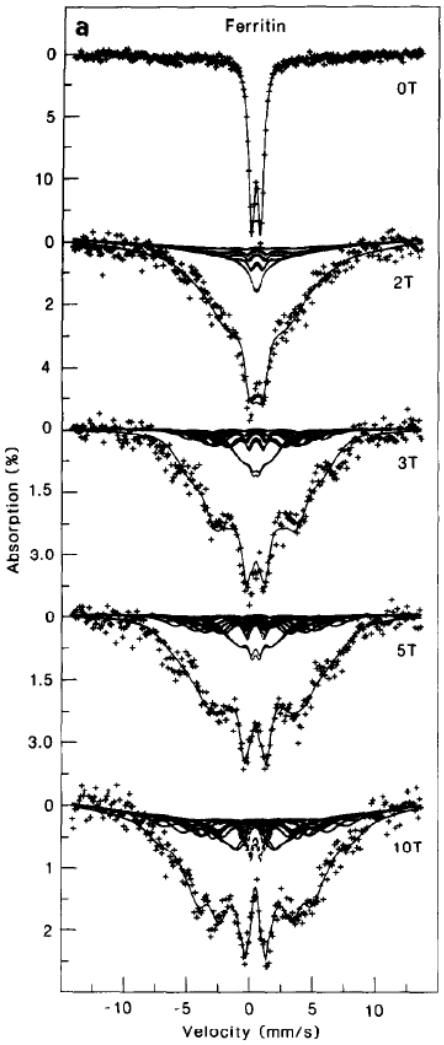

Figure 6. Mössbauer spectra of human spleen ferritin at 100 K obtained in the indicated applied magnetic fields. Reprinted with permission from [88]. Copyright 1987 by Elsevier.

consists of a doublet, indicating that the particles are superparamagnetic at this temperature, but a magnetic splitting is induced when external magnetic fields are applied. The saturation hyperfine field in ferritin is of the order of 45 T, corresponding to a splitting of lines 1 and 6 in the spectrum around 15 mm s^{-1}. The figure shows that even at the largest applied fields, the average magnetic hyperfine splitting is much smaller, indicating that the particles are far from being magnetically saturated. The analysis of the spectra of antiferromagnetic nanoparticles in applied fields is much more complex than that of the corresponding spectra of ferromagnetic and ferrimagnetic nanoparticles. For small applied fields, the anisotropy energy may be large compared to the Zeeman energy, and therefore the relaxation takes place between two minima with different energies, which depend on the size and direction of the applied field. At large applied fields, this model may not be appropriate, because the Zeeman and the anisotropy

energies may be comparable. Because of these complications it is not straightforward to obtain reliable values for the magnetic moments from such Mössbauer measurements on antiferromagnetic nanoparticles [53, 88].

4.3. Neutron scattering studies

Neutron scattering is another technique that is useful for studies of time-dependent phenomena. Magnetic dynamics in solids can be studied by inelastic neutron scattering. In such studies, one can measure, for example, the energy distribution of neutrons that are diffracted at a wavevector corresponding to a magnetic diffraction peak. This gives information about magnetic excitations, such as spin waves, and in studies of magnetic nanoparticles this technique can give information on both superparamagnetic relaxation and uniform magnetic excitations [24, 25]. The timescale of neutron scattering is much shorter than that of Mössbauer spectroscopy. Therefore, neutron scattering makes it possible to study details of magnetic fluctuations that are not revealed in Mössbauer spectroscopy and magnetization measurements. For example, neutron scattering can be used to estimate the energy related to transitions between uniform precession states, whereas Mössbauer spectroscopy only allows measurement of a magnetic hyperfine field that is averaged over all magnetic fluctuations. Before discussing neutron data, it is useful to look in more detail at magnetic excitations in nanoparticles.

For a cubic ferromagnetic or ferrimagnetic material with lattice constant a, the dispersion relation for spin waves for which $aq \ll 1$ can be written [3, 19, 89, 90] as

$$\hbar\omega_q = Dq^2 + g\mu_B B_A, \tag{10}$$

where ω_q is the angular frequency of a spin wave with wavevector q, D is the exchange stiffness constant, g is the Landé factor, μ_B is the Bohr magneton and $B_A = 2K/M$ is the anisotropy field with M being the magnetization. In nanoparticles with cubic shape, in which surface effects are neglected, the allowed values of the wavevector are given by [19, 91]

$$q = n\pi/d, \qquad n = 0, 1, 2, 3 \ldots \tag{11}$$

where d is the side length. Similar quantization of the spin wave spectrum can be found also in real nanoparticles [92]. Because of this quantization, there are in very small particles large energy gaps between the uniform ($n = 0$) mode and the modes with $n > 0$. Therefore, spin waves with $q = 0$ are predominant in nanoparticles, and the first term in equation (10) can often be neglected [19]. In many theoretical investigations of magnetic excitations in nanoparticles, the $q = 0$ mode has been neglected, and the calculations therefore only give information on the modes with $q > 0$. However, if a sufficiently large magnetic field is applied, the excitations of the uniform mode are suppressed, and the magnetic dynamics can then be dominated by modes with $q > 0$ [91]. The z-components of the magnetic moments of neighbouring precession states of the uniform mode, with slightly different precession angles, differ by $g\mu_B$ [22]. In inelastic neutron spectra, the uniform mode gives rise to separate peaks at energies corresponding to the energy difference, ε_0, between neighbouring precession states. In ferromagnetic and ferrimagnetic nanoparticles this energy difference is given by [19, 25]

$$\varepsilon_0 = \hbar\omega_0 = g\mu_B B_A. \tag{12}$$

Typically, B_A is of the order of 0.1 T, corresponding to $\varepsilon_0 \approx 0.01$ meV. Thus, the peaks are hard to observe in a typical neutron spectrometer with an energy resolution of the order of 0.1 meV [25]. However, if a large magnetic field, $B_{ext} \gg B_A$, is applied, the energy difference is given by

$$\varepsilon_0 \approx g\mu_B B_{ext} \tag{13}$$

and the inelastic peaks may then be visible for applied fields larger than $\sim$1 T [25].

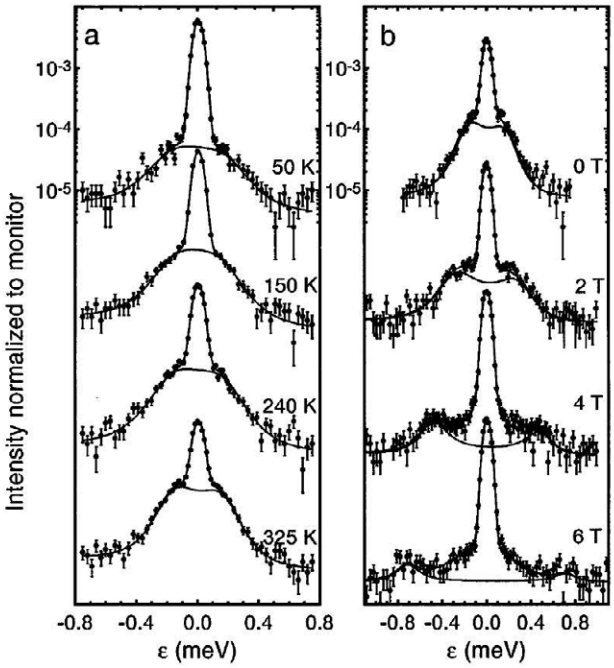

Figure 7. Inelastic neutron scattering data for 15 nm hematite nanoparticles. (a) Data obtained at zero applied magnetic field at the indicated temperatures. (b) Data obtained at 268 K at the indicated applied magnetic fields. Reprinted with permission from [24]. Copyright 1997 by the American Physical Society.

In antiferromagnetic nanoparticles the situation is different because the dispersion relation for spin waves is given by the more complex expression [22]

$$\hbar\omega_q = g\mu_B[(B_E + B_A)^2 - B_E^2(1 - Cq^2)]^{1/2}. \tag{14}$$

Here $B_A = K/M_S$ is the anisotropy field for an antiferromagnet with sublattice magnetization M_S, B_E is the exchange field and C is a constant. Thus, in nanoparticles, in which the uniform mode is predominant, the energy difference between neighbouring precession states, for $B_E \gg B_A$, is given by [93, 94]

$$\varepsilon_0 = \hbar\omega_0 \approx g\mu_B\sqrt{2B_E B_A}. \tag{15}$$

The exchange field may be up to around 1000 T and the energy, ε_0, of the uniform mode in antiferromagnetic nanoparticles can therefore be much larger than that of ferromagnetic and ferrimagnetic nanoparticles and can more easily be observed in inelastic neutron scattering experiments in zero applied field.

As an example, we consider inelastic neutron scattering studies of 15 nm α-Fe_2O_3 nanoparticles from the same batch as the sample used for the neutron and x-ray diffraction data in figure 1 and the Mössbauer spectra in figure 4. The energy distribution of neutrons scattered at $Q = 1.37$ Å^{-1}, corresponding to the (003) peak, is shown in figure 7 [24]. Data are displayed for different temperatures and applied magnetic fields. The neutron data in figure 7(a) show a relatively narrow, quasielastic line, centred at energy $\varepsilon = 0$ meV. On both sides of this quasielastic line, inelastic lines can be seen with an intensity that increases with increasing temperature. The energy distribution (apart from background terms) can be

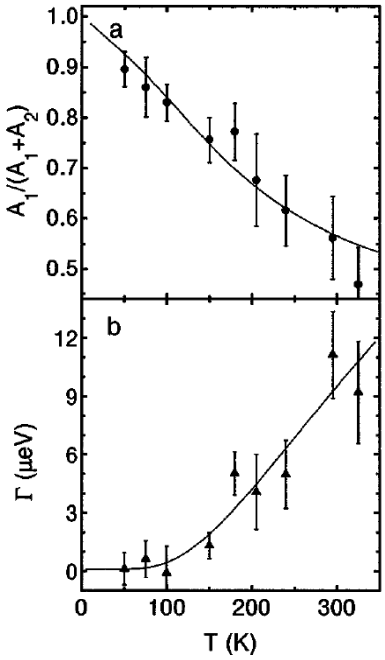

Figure 8. Parameters obtained from fits of the inelastic neutron data shown in figure 7(a). (a) Relative area of the quasielastic peaks. (b) Superparamagnetic relaxation parameter Γ obtained from the line width of the quasielastic peak. Reprinted with permission from [24]. Copyright 1997 by the American Physical Society.

described by [24, 95, 96]

$$I(\varepsilon) = \frac{A_1}{\pi} D(\varepsilon) \frac{\Gamma}{\varepsilon^2 + \Gamma^2} + \frac{A_2}{\pi} D(\varepsilon) \frac{2\gamma\varepsilon_0^2}{(\varepsilon^2 - \varepsilon_0^2)^2 + 4\gamma^2\varepsilon^2}, \tag{16}$$

where A_1 is the area of the quasielastic peak and A_2 is the area of the inelastic components. $\pm\varepsilon_0$ are the positions of the inelastic peaks, γ is the width of these peaks and Γ is the width of the quasielastic peak. $D(\varepsilon)$ is the detailed balance factor due to the difference in the population of the creation and annihilation states of the uniform excitations. Due to the presence of adsorbed water on the surface of the particles there is a strong incoherent elastic signal increasing the signal at $\varepsilon = 0$ meV. Before comparing with experimental data, the sum of $I(\varepsilon)$ and the incoherent signal must be convoluted with the experimental resolution function. Some of the parameters, derived from fits to the zero-field experimental data of figure 7(a), are shown in figure 8. The relative area of the inelastic peaks is proportional to $\langle \sin^2 \theta \rangle$ and therefore it increases with temperature. At low temperatures the area ratio is given by

$$\frac{A_1}{A_1 + A_2} \approx 1 - \frac{k_B T}{KV}. \tag{17}$$

The fit to the temperature dependence of $A_1/(A_1 + A_2)$, shown in figure 8(a), was obtained using a more exact analytical expression [24], and the value $KV/k_B \approx 700$ K was obtained. The width of the quasielastic line increases with increasing temperature due to superparamagnetic relaxation as seen in figure 8(b), and the line broadening is inversely proportional to the superparamagnetic relaxation time, $\Gamma = h/\tau$ [95]. From the temperature dependence of Γ, the values $KV/k_B \approx 500$ K and $\tau_0 \approx 1.4 \times 10^{-11}$ s were estimated [95].

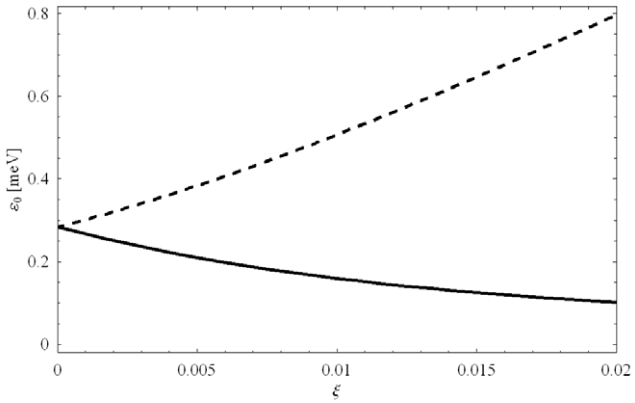

Figure 9. Energy of the uniform mode as a function of the uncompensated magnetic moment of antiferromagnetic nanoparticles. The lines were calculated using equation (18) with $B_A = 0.01$ T and $B_E = 300$ T. Reprinted with permission from [63]. Copyright 2006 by the American Physical Society.

The values of magnetic anisotropy energy and τ_0, obtained from neutron scattering, are in good agreement with those obtained from the Mössbauer studies (section 4.1).

The inelastic neutron data in figure 7(b), measured at 260 K in various applied magnetic fields, show that the inelastic peaks are shifted to larger energies when the field is increased with a related decrease of the relative area. The field dependence of ε_0 at high fields was found to be in accordance with equation (13), with $g \cong 2$ as expected for Fe^{3+} [24].

The expression for the energy of the uniform mode in an antiferromagnet (equation (15)) was derived for a perfect two-sublattice antiferromagnet with anisotropy energy given by equation (1), i.e., the existence of an uncompensated magnetic moment, μ_u, was not taken into account. It is, however, noteworthy that even a small difference in the sublattice magnetic moments can have an influence on the value of ε_0. An antiferromagnetic nanoparticle with an uncompensated magnetic moment should in principle be considered as a ferrimagnet with a small difference between the values of the sublattice magnetizations, and equation (15) should then be replaced by [93, 97–100]

$$\varepsilon_0^{\pm} = \tfrac{1}{2} g \mu_B B_E (\sqrt{4\lambda^2 + 4\lambda(2+\xi) + \xi^2} \pm \xi). \tag{18}$$

Here, $\lambda = B_A/B_E$ and $\xi = \mu_u/(M_S V)$ is the ratio of the uncompensated moment and the sublattice magnetic moment. Thus, instead of the single mode in the ideal antiferromagnet with energy given by equation (15), there are now two modes with energies that depend on the magnitude of the uncompensated magnetic moment. The dependence of $\varepsilon_0^{\pm}$ on the value of ξ, calculated by use of equation (18), is shown in figure 9. Because of the different thermal populations of the two modes, the low-energy mode will give the predominant contribution to the magnetic dynamics. Even small values of the uncompensated moment can result in significant changes of the energies. For example, a value of ξ around 0.01 reduces the energy of the low-energy mode by a factor of about two. Since the value of ξ in general is expected to increase with decreasing particle size, the effect should be largest in very small particles. In accordance with this, it has been found that the effect is insignificant in 15 nm α-Fe_2O_3 nanoparticles, but clearly visible in 8 nm α-Fe_2O_3 nanoparticles [99].

The use of the anisotropy energy given by equation (1) is only a rough approximation for α-Fe_2O_3 nanoparticles, because the particles have both a small in-plane anisotropy and a larger out-of-plane anisotropy. If this is taken into account, one finds that there are two different uniform modes even in the absence of an uncompensated moment. The inelastic

neutron scattering data, shown in figure 7, give information about a low-energy uniform mode, which is characterized by an elliptic precession very close to the (001) plane, and the parameters obtained from this mode give information on the in-plane anisotropy. It has been shown [49] that inelastic neutron data for neutrons scattered at $Q = 1.50$ Å^{-1} give information about a high-energy uniform mode, which is characterized by fluctuations out of the plane. Neutron data therefore make it possible to estimate the values of both the in-plane and the out-of-plane anisotropy constants [49].

NiO particles also have a small in-plane anisotropy, but a much larger out-of-plane anisotropy. In this case the energies of the uniform modes are less dependent on the magnitude of the uncompensated moment [100]. The energy of the low-energy uniform mode of NiO nanoparticles, estimated from inelastic neutron scattering experiments, was considerably smaller than predicted by equation (15), when inserting the bulk exchange field and an anisotropy field derived from the temperature dependence of the relative area of the inelastic peaks [100]. This suggests that the effective exchange field in the nanoparticles is smaller than the bulk value, as studies of the spin–flop transition in α-Fe_2O_3 nanoparticles also have suggested [51].

4.4. The uniform mode in antiferromagnetic nanoparticles and thermoinduced magnetization

In early studies of superparamagnetism [17, 18] and collective magnetic excitations [20, 21], ferromagnetic, ferrimagnetic and antiferromagnetic particles were all treated as classical spins, i.e., it was assumed that the total spin of a particle was so large that quantization could be neglected. This is a good approximation for ferromagnetic and ferrimagnetic particles for which the total spin S typically is of the order of 10^3–10^5. When the uniform mode is excited, the possible values of the z-component of the spin are $S_z = S, S-1, S-2, \ldots, -(S-2), -(S-1), -S$, i.e., there are $2S+1$ precession states with z-components of the magnetic moments given by $g\mu_B S_z$. This results in the energy differences between neighbouring states given by equations (12) and (13).

In ferromagnetic nanoparticles all ionic spins precess in parallel in the uniform mode. However, in antiferromagnetic nanoparticles the two sublattices are not strictly antiparallel when the uniform mode is excited, but form different angles θ_A and θ_B with the easy axis [93, 94], as illustrated in figure 10. These different precession angles result in a contribution to the magnetic moment of the particle. For simplicity, we first consider an antiferromagnetic nanoparticle with magnetic anisotropy energy given by equation (1) and without an uncompensated magnetic moment. For a particle with $B_A \ll B_E$ the two angles are related by [19, 101]

$$\frac{\sin\theta_A}{\sin\theta_B} = 1 \pm \delta, \tag{19}$$

where

$$\delta \approx \sqrt{\frac{2B_A}{B_E}}. \tag{20}$$

The number of precession states in an antiferromagnetic nanoparticle is determined by the fact that the difference in magnetic moments of neighbouring precession states is given by $g\mu_B$ [19]. Because the differences between the precession angles and θ_B are small, the number of precession states in an antiferromagnetic nanoparticle is much smaller than the corresponding number of states in a ferromagnetic nanoparticle (by a factor of the order of δ [19]). For this reason the temperature dependence of the average hyperfine field deviates from equation (3) at low temperatures due to quantum effects [19].

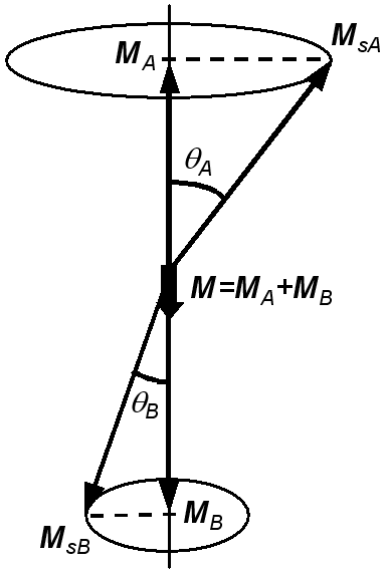

Figure 10. Schematic illustration of the uniform mode in nanoparticles of antiferromagnetic nanoparticles. Reprinted with permission from [62]. Copyright 2004 by the American Physical Society.

The magnetic moment due to the different precession angles (the thermoinduced moment) has at low temperatures an absolute value given by [19]

$$|\mu_t| = M_S V |\cos\theta_A - \cos\theta_B| \approx M_S V \delta \sin^2\theta_B. \tag{21}$$

In zero applied field, precession states with magnetic moments up and down are degenerate, and the average magnetic moment is therefore zero, but the average of the absolute value of μ_t is given by [19, 62]

$$\langle|\mu_t|\rangle \approx \frac{2k_B T}{\sqrt{2B_A B_E}}. \tag{22}$$

Thus, the absolute value of the moment increases linearly with temperature and the thermoinduced moment is independent of the particle volume. This can be deduced from equation (21), since $\langle\sin^2\theta_B\rangle$ is inversely proportional to the volume, V [19].

In an applied magnetic field the degeneracy is lifted, and therefore a finite magnetization can be observed. The initial susceptibility due to the thermoinduced magnetization is given by [19, 62]

$$\chi_i = \frac{4\mu_0}{V}\frac{k_B T}{B_A B_E}, \tag{23}$$

i.e., the initial susceptibility also increases linearly with temperature.

Because nanoparticles of antiferromagnetic materials usually also have an uncompensated magnetic moment, μ_u, the initial susceptibility will have a contribution related to μ_u and is then given by [63]

$$\chi_i \approx \frac{\mu_0}{V}\left(\frac{\mu_u^2}{k_B T} + \frac{4k_B T}{B_A B_E}\right). \tag{24}$$

According to equation (24), the contribution to the initial susceptibility due to thermoinduced magnetization will be predominant for $T > \mu_u\sqrt{B_A B_E}/2k_B$.

4.5. Macroscopic quantum tunnelling

Thermally activated magnetization reversal is a well established phenomenon, which has been studied by a number of experimental techniques [1]. It has, however, been suggested that macroscopic quantum tunnelling between the minima of the anisotropy energy also may take place [102–104]. Below a crossover temperature, the relaxation due to quantum tunnelling should be predominant and the relaxation should therefore be independent of temperature. Theoretical investigations have shown that such macroscopic quantum tunnelling should be easier to detect in antiferromagnetic nanoparticles than in ferromagnetic and ferrimagnetic particles [103, 104].

Several experimental studies of ferromagnetic, ferrimagnetic and antiferromagnetic nanoparticles have indicated a temperature-independent relaxation below a crossover temperature of the order of 1 K [105–108]. This may be ascribed to macroscopic quantum tunnelling. However, it has been suggested that thermoinduced magnetization also can contribute to a temperature-independent relaxation [62]. It has also been pointed out that an apparent temperature independence of the relaxation time at low temperatures could be due to a distribution of energy barriers, ΔE, which diverges for $\Delta E \rightarrow 0$ [109]. Both experimental [110] and theoretical [31, 76, 111] investigations have shown that such distributions of energy barriers can be found in magnetic nanoparticles.

5. Magnetic interactions between antiferromagnetic nanoparticles

The superparamagnetic relaxation of nanoparticles is very sensitive to interparticle interactions. Experimental studies of frozen suspensions of ferromagnetic and ferrimagnetic nanoparticles have shown that magnetic dipole interactions can lead to a divergence of the relaxation time at a finite temperature, such that equation (2) may be replaced by a Vogel–Fulcher law [112] or by an expression based on spin-glass models [113]. The critical temperature at which the relaxation time diverges is of the order of [114]

$$T_{\mathrm{p}} \approx \frac{\mu_0}{4\pi k_{\mathrm{B}}} \frac{\mu^2}{d_{\mathrm{p}}^3}, \tag{25}$$

where d_{p} is the average distance between the particles. Thus, T_{p} increases with increasing concentration of particles in the suspensions. Below the critical temperature, the samples may have magnetic properties, which have similarities to those of spin-glasses [113–116].

The magnetic moments of antiferromagnetic nanoparticles are typically much smaller than those of ferromagnetic and ferrimagnetic nanoparticles, and therefore the dipole interactions are insufficient to significantly affect the superparamagnetic relaxation [117]. In fact, the dipole interactions between antiferromagnetic nanoparticles in close proximity are typically so small that the related critical temperature is well below 1 K. For example, for particles with magnetic moments of the order of 300 μ_{B} (typical for ferritin [58, 59]) and with an average centre to centre distance of 8 nm (corresponding to the diameter of typical ferritin cores) the critical temperature, estimated from equation (25), is of the order of 0.2 K. For 20 nm hematite particles, which have a magnetic moment due to its canted spin structure, one finds that even if the particles are in close proximity, the value of T_{p} is also of the order of 0.2 K [117]. Nevertheless, in several experimental studies of samples of uncoated antiferromagnetic nanoparticles, it has been found that aggregation can change the magnetic dynamics drastically. For instance, the temperature where the particles become superparamagnetic can increase by more than 100 K [117–119]. It has been concluded that exchange interaction between surface ions of neighbouring particles is responsible for the effect. This implies that the particles are

in such close proximity that the electronic wavefunctions of atoms at the interfaces overlap. Because the dipole interactions can be considered negligible in samples of antiferromagnetic nanoparticles, such samples present a unique possibility to study exchange coupling between magnetic nanoparticles.

The magnetic energy of a particle, p, which interacts with its neighbour particles, q, may be written as [21, 99, 117, 120, 121]

$$E_i = KV_p \sin^2\theta - \vec{M}_p \cdot \sum_q J_{pq}\vec{M}_q, \tag{26}$$

where $\vec{M}_p$ and $\vec{M}_q$ represent the (sublattice) magnetization of the particles p and q, respectively, and J_{pq} is an effective exchange coupling constant due to exchange coupling between surface atoms belonging to the neighbouring particles. The summation in the last term may be considered as an effective interaction field. If the first term in equation (26) is predominant, superparamagnetic relaxation may take place between the easy directions close to $\theta = 0$ and π. However, if the interaction is significant, the energy at the two minima will differ and the thermal populations will therefore also differ. For strong interactions, there may be only one energy minimum. At finite temperatures, the sublattice magnetization vectors will mainly fluctuate around the direction corresponding to the lower energy minimum. If the fluctuations of the sublattice magnetization directions are fast compared to the timescale of Mössbauer spectroscopy, the magnetic splitting in the spectra will be proportional to the average hyperfine field. Variations of the magnitude and direction of the interaction field in the sample result in a distribution of magnetic hyperfine splittings, which leads to spectra with broadened sextets.

The interactions between nanoparticles can often be modified by varying the preparation technique. Samples of non-interacting or weakly interacting particles can be obtained by coating the particles with, for example, oleic acid. Samples of strongly interacting particles may be obtained by drying, for example, suspensions of uncoated α-Fe_2O_3 nanoparticles. Figures 11(a) and (b) show Mössbauer spectra of coated (weakly interacting) and uncoated (strongly interacting) 20 nm α-Fe_2O_3 particles, respectively [117]. The spectra of the coated nanoparticles (figure 11(a)) show the typical behaviour of non-interacting magnetic nanoparticles, i.e., the simultaneous presence of a doublet and a sextet with a temperature-dependent area ratio over a broad range of temperatures. Around 240 K, the sextet vanishes and only a doublet is present, indicating that all particles exhibit fast superparamagnetic relaxation above this temperature. The spectra of the interacting particles (figure 11(b)) show a completely different evolution with increasing temperature. Instead of the appearance of a doublet, the spectra show a substantial asymmetric broadening of the lines of the sextet, and even at 360 K there is no visible doublet. As discussed above, this is typical for Mössbauer spectra of interacting particles with a distribution of interaction fields. Thus, the large differences between the spectra in figures 11(a) and (b) illustrate the importance of interparticle interactions in samples of antiferromagnetic nanoparticles. The spectra of the interacting particles in figure 11(b) have similarities to the spectrum of superparamagnetic particles at 240 K in an applied field (figure 11(a), bottom). This is in accordance with the description of the influence of interactions in terms of an effective interaction field. From an analysis of the temperature dependence of the hyperfine field distribution, the effective interaction energy and the magnetic anisotropy constant could be determined [117].

The collective magnetic excitations can also be suppressed by interparticle interactions, and the expression for the average magnetic hyperfine field (equation (3)) may then be replaced by [21, 117, 121]

$$B_{\text{obs}} \approx B_0\left[1 - \frac{k_{\text{B}}T}{2KV + E_{\text{int}}}\right], \tag{27}$$

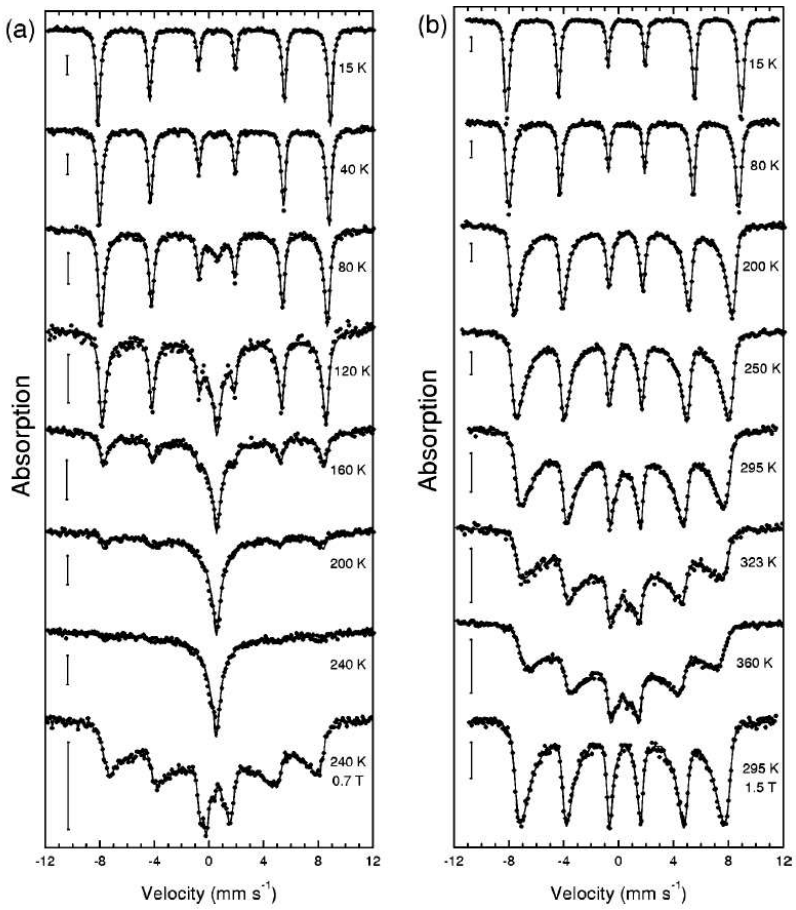

Figure 11. Mössbauer spectra of coated (weakly interacting) (a) and uncoated (strongly interacting) (b) 20 nm hematite nanoparticles obtained at the indicated temperatures [117]. Reprinted with permission from [117]. Copyright 2000 by the American Physical Society.

where E_{int} is related to the strength of the interparticle interactions. Figure 12 shows the temperature dependence of the magnetic hyperfine fields at low temperatures of 8 nm non-interacting and interacting α-Fe_2O_3 nanoparticles [122]. The linear temperature dependence of the data is in accordance with equations (3) and (27). Assuming that the anisotropy energy constants are identical for the particles of the two samples, an effective interaction energy, $E_{\text{int}}/k_{\text{B}} \approx 1300$ K could be estimated from the slopes of the curves in figure 12.

Figure 13 shows inelastic neutron scattering data at $Q = 1.37$ Å^{-1} for weakly and strongly interacting 8 nm α-Fe_2O_3 nanoparticles [99]. The data, obtained in zero applied magnetic field for weakly (a) and strongly (c) interacting particles, show that strong interactions shift the positions of the inelastic peaks to higher energies, but their relative areas decrease. The interactions affect both the excitation energy and the area ratio in a way that is similar to the effect of an applied field (figure 13(b)). Similar results have been found in an inelastic neutron scattering study of NiO nanoparticles [100].

Recent neutron diffraction experiments [123] have shown that α-Fe_2O_3 nanoparticles prepared by a gel–sol method may be attached in such a way that neighbouring particles have a common crystallographic orientation and a magnetic correlation in the [001]

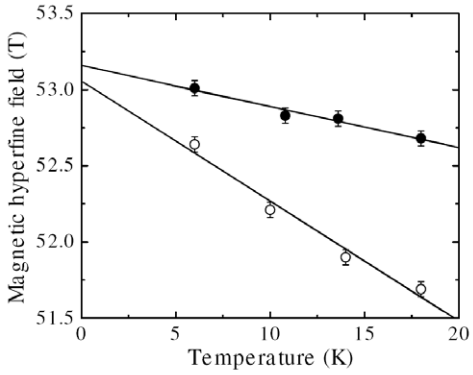

Figure 12. Magnetic hyperfine field of coated (open circles) and uncoated 8 nm hematite nanoparticles obtained from low-temperature Mössbauer spectra. The lines are linear fits to the data extrapolated to $T = 0$ K. Reprinted with permission from [122]. Copyright 2005 by the American Physical Society.

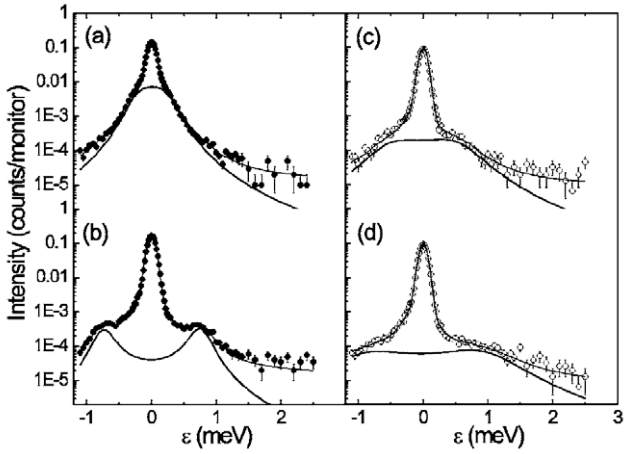

Figure 13. Inelastic neutron data for 8 nm α-Fe_2O_3 nanoparticles. Data for coated nanoparticles in (a) zero field and (b) in an applied field of 6 T, respectively. Data for uncoated nanoparticles in (c) zero field and (d) in an applied field of 6 T, respectively. Reprinted with permission from [99]. Copyright 2006 by the American Physical Society.

direction. Figure 14(a) shows neutron diffraction data for such a sample of 8 nm α-Fe_2O_3 nanoparticles [123]. Most of the diffraction lines have line widths that are considerably larger than the instrumental broadening, but in accordance with the particle size estimated from x-ray diffraction data and electron micrographs. However, the width of the magnetic (003) reflection is considerably narrower than that of the other peaks. This peak could be well fitted with two components, one with a line width corresponding to a particle size of about 8 nm and another with a relative area of about 36% and a width corresponding to a correlation length of $\sim$22 nm. This suggests that about a third of the particles are present in chains with around three particles that show oriented attachment such that both the crystallographic and the magnetic order continue across the interfaces. High-resolution electron microscopy studies confirmed the existence of such chains of particles with a common crystallographic orientation [123].

Mössbauer studies of interacting α-Fe_2O_3 nanoparticles have also shown that the interactions between particles with different relative crystallographic orientations can lead to

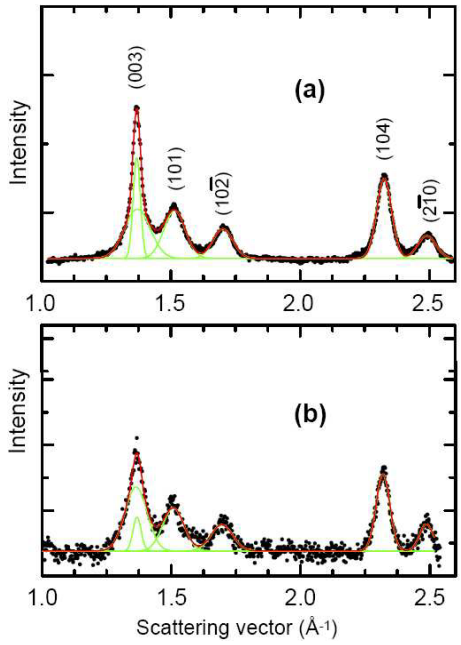

Figure 14. Neutron diffraction data for 8 nm hematite particles obtained at room temperature. (a) Data for the as-prepared (strongly interacting) sample. (b) Data for the ground sample. Reprinted with permission from [123]. Copyright 2005 by the American Physical Society.

(This figure is in colour only in the electronic version)

a rotation of the sublattice magnetization directions [122]. In the spectra of α-Fe_2O_3, there is a small quadrupole shift, ε_{qs}, because of the non-cubic environments of the iron ions, which give rise to an electric field gradient along the [001] direction. In general, the quadrupole shift in a Mössbauer spectrum depends on the angle α between the electric field gradient and the magnetic hyperfine field according to the expression

$$\varepsilon_{qs} = \varepsilon^0_{qs}(3\cos^2\alpha - 1)/2, \tag{28}$$

where $\varepsilon^0_{qs} = 0.20$ mm s^{-1} in α-Fe_2O_3. Below the Morin transition temperature, the magnetic hyperfine field is parallel to the electric field gradient, and the quadrupole shift is therefore 0.20 mm s^{-1}. Above the Morin transition in bulk α-Fe_2O_3 and in non-interacting nanoparticles at all temperatures, the magnetic hyperfine field is perpendicular to the electric field gradient and the quadrupole shift is then -0.1 mm s^{-1}. However, in samples of interacting α-Fe_2O_3 nanoparticles the quadrupole shift can deviate from this value. Figure 15 shows the quadrupole shift of non-interacting and interacting 8 nm α-Fe_2O_3 nanoparticles as a function of temperature. For the non-interacting nanoparticles, the quadrupole shifts are close to -0.10 mm s^{-1}, but the interacting nanoparticles show quadrupole shifts of the order of -0.07 to -0.08 mm s^{-1}, indicating that the value of α differs from 90° and rather is of the order of 75°. This can be explained by rotation of the sublattice magnetization directions induced by the exchange interactions between neighbouring particles with different crystallographic orientation [122].

It is also noteworthy that the extrapolations of the temperature dependence of the hyperfine fields to $T = 0$ K differ for the non-interacting and the interacting nanoparticles (figure 12). This is in accordance with a rotation of the sublattice magnetization directions, because the contribution to the magnetic hyperfine field from the dipole fields of neighbouring magnetic

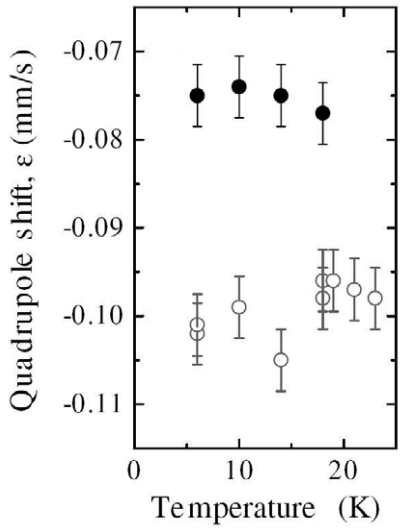

Figure 15. Quadrupole shift of coated (weakly interacting) (open circles) and uncoated (strongly interacting) (solid circles) 8 nm hematite nanoparticles as a function of temperature. Reprinted with permission from [122]. Copyright 2005 by the American Physical Society.

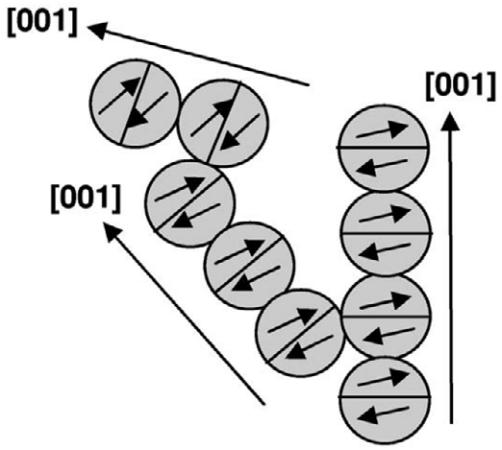

Figure 16. Schematic illustration of a network of interacting α-Fe_2O_3 nanoparticles. Reprinted with permission from [123]. Copyright 2005 by the American Physical Society.

ions depends on the angle between the sublattice magnetization and the [001] direction in α-Fe_2O_3 [124]. The measured difference between the extrapolated hyperfine fields was in accordance with the rotation angle obtained from the analysis of the quadrupole shift [122].

It is likely that the strong suppression of superparamagnetic relaxation in samples of agglomerated α-Fe_2O_3 nanoparticles is governed by larger networks of interacting particles with both parallel and non-parallel [001] axes [122, 123]. Figure 16 shows a schematic illustration of such a network [123]. Here particles are attached in small chains with parallel [001] axes, but the neighbouring chains or particles may have different orientations of their [001] axes. This model describes most of the measured features well.

The establishment of strong interactions between α-Fe_2O_3 nanoparticles is a reversible process [125]. Exposure of an agglomerated sample of 8 nm α-Fe_2O_3 particles in water to ultrasound can result in a change of the Mössbauer spectrum from a sextet with broadened lines to a doublet, but after subsequent drying, the sextet can be re-established. Several Mössbauer studies have shown that gentle grinding of samples of interacting α-Fe_2O_3 particles also can lead to a significant reduction of the interactions [123, 125, 126]. The neutron diffraction studies of 8 nm α-Fe_2O_3 nanoparticles (figure 14) showed that the narrow (003) reflection of interacting particles (figure 14(a)) became broader and had a width comparable to that of the other reflections after gentle grinding (figure 14(b)). Thus, the oriented attachment seems to have been destroyed by the grinding.

Goethite (α-FeOOH) is a common mineral and it is usually poorly crystalline, both when formed in nature and when synthesized in the laboratory. Well crystallized goethite has a Néel temperature around 393 K [120]. Mössbauer spectra of goethite commonly show sextets with asymmetrically broadened lines with average hyperfine fields much smaller than the bulk value. Only in a small temperature range does a doublet coexist with the sextet. The temperature dependence of the average hyperfine field of goethite nanoparticles has been found to be in accordance with a simple mean-field model for interacting particles [120]. It has been suggested [127] that goethite particles consist of smaller, interacting clusters, and that the spectra may explained by a distribution of precession states in the clusters with different precession angles, which give rise to different hyperfine fields. In this model, transitions between the precession states were neglected, and this may not be realistic [117]. Recent studies have shown that goethite particles may grow via oriented attachment [128–130], and this suggests that goethite particles in fact may consist of smaller interacting clusters. The different interpretations have given rise to some debate in the literature [117, 127, 131].

Interactions between NiO nanoparticles have been studied by electron magnetic resonance [132] and by DC and AC magnetization measurements [133]. As in the case of α-Fe_2O_3 nanoparticles, it was found that the superparamagnetic relaxation to a large extent was suppressed in samples of uncoated particles in comparison with particles coated with oleic acid. Mössbauer studies of nanoparticles of ^{57}Fe-doped NiO, prepared by heat treatment of $Ni(OH)_2$, showed similar effects [118]. It has also been found that interparticle interactions between NiO nanoparticles can be reduced by grinding the samples or by exposing them to ultrasound [134]. Even suspension in water or long-term exposure to air leads to reduction of the interparticle interactions. However, unlike α-Fe_2O_3 nanoparticles, the strong interactions could not be re-established by drying suspensions of weakly interacting NiO nanoparticles. It is likely that the different behaviour of α-Fe_2O_3 and NiO nanoparticles can be explained by differences in the affinity of the particles to water [134]. Adsorption of water on the surface of the NiO particles may prevent the formation of strong exchange bonds between the particles, reducing the interactions between particles.

Mössbauer studies have shown that interactions between nanoparticles of different antiferromagnetic materials can have unexpected effects on the magnetic properties [119]. For example, the superparamagnetic relaxation of 9 nm α-Fe_2O_3 particles was to a large extent suppressed when they were mixed with nanoparticles of CoO, whereas the opposite effect was found when the iron oxide particles were mixed with nanoparticles of NiO. The different influence of CoO and NiO particles may be explained by the smaller magnetic anisotropy of the NiO nanoparticles [119], but a large affinity of NiO to water may also contribute to a reduction of the interactions. In samples of mixtures of α-Fe_2O_3 and NiO nanoparticles, it was surprisingly found that a Morin transition took place although there was no Morin transition in the sample consisting solely of the α-Fe_2O_3 nanoparticles [119]. Mixtures of antiferromagnetic nanoparticles with ferromagnetic or ferrimagnetic nanoparticles with strong

interparticle interactions have shown exchange bias and enhanced coercivity [13–16, 135]. Such nanocomposites may therefore have applications as permanent magnets. In a recent study of core–shell Co–CoO nanoparticles it was shown that exchange interactions between the antiferromagnetic CoO shells of neighbouring particles can have a significant effect on the blocking temperature, the coercivity and the exchange bias [136].

6. Summary

The size dependence of the magnetic properties of nanoparticles of antiferromagnetic materials is in many respects substantially different from that of nanoparticles of ferromagnetic and ferrimagnetic materials. The magnetic moment of a nanoparticle of a ferromagnetic or ferrimagnetic material is basically determined by the particle volume and the magnetization, which may be similar to the bulk value, although surface effects and defects often result in a (slightly) smaller magnetization. In contrast, the magnetic moment of an antiferromagnetic nanoparticle is mainly a result of imperfections or finite-size effects, e.g., different numbers of spins in the sublattices, which lead to an uncompensated moment and a related increase of the saturation magnetization with decreasing particle size, but thermoinduced magnetization is also expected to give a contribution to the moment of very small particles.

The small magnetic moments of antiferromagnetic nanoparticles makes the analysis of magnetization and in-field Mössbauer data much less straightforward than the analysis of data for ferromagnetic and ferrimagnetic nanoparticles. This is because the isothermal magnetization curves of particles with very small moments are often far from saturation in the superparamagnetic regime. Furthermore, the anisotropy may be large compared to the Zeeman energy, such that the Langevin function is not a good approximation to the magnetization curves.

As in ferromagnetic and ferrimagnetic nanoparticles, the magnetic excitations of antiferromagnetic nanoparticles at low temperatures are dominated by the uniform excitations ($q = 0$ spin waves). This leads to a linear decrease of the sublattice magnetization with increasing temperature and a small net magnetic moment that increases with increasing temperature. The excitation energy of the uniform mode in antiferromagnetic nanoparticles is much larger than that of ferromagnetic and ferrimagnetic nanoparticles, but even a small uncompensated moment can have a significant influence on the excitation energy.

Interactions between nanoparticles can have a large influence on the magnetic dynamics, e.g., the superparamagnetic relaxation. The dipole interaction between antiferromagnetic nanoparticles in close proximity is insignificant; therefore, the effects must be explained by exchange interaction between surface atoms of neighbouring nanoparticles. This exchange interaction can to a large extent be varied by exposing the samples to appropriate macroscopic treatments such as gentle grinding or exposure to ultrasound. It has been found that nanoparticles of α-Fe_2O_3 can be attached in such a way that the crystallographic and magnetic order continue across the interfaces. Interactions between antiferromagnetic nanoparticles with different crystallographic orientations can result in rotation of the sublattice magnetization directions.

References

[1] Dormann J L, Fiorani D and Tronc E 1997 *Adv. Chem. Phys.* **98** 283
[2] Dormann J L and Fiorani (ed) 1992 *Magnetic Properties of Fine Particles* (Amsterdam: North-Holland)
[3] Kodama R H 1999 *J. Magn. Magn. Mater.* **200** 359
[4] Fiorani D (ed) 2005 *Surface Effects in Magnetic Nanoparticles* (New York: Springer)
[5] Zhu J-G 2003 *Mater. Today* **6** 22
[6] Pankhurst Q A, Conolly J, Jones S K and Dobson J 2003 *J. Phys. D: Appl. Phys.* **36** R167

[7] Tartaj P, del Puerto Morales M, Veintemillas-Verdaguer S, Gonzalez-Carreno T and Serna C J 2003 *J. Phys. D: Appl. Phys.* **36** R182
[8] Holm C and Weis J-J 2005 *Curr. Opin. Colloid Interface Sci.* **10** 133
[9] Nogués J and Schuller I K 1999 *J. Magn. Magn. Mater.* **192** 203
[10] Berkowitz A E and Takano K 1999 *J. Magn. Magn. Mater.* **200** 552
[11] Comstock R L 2002 *J. Mater. Sci. Mater. Electron.* **13** 509
[12] Skumryev V, Stoyanov S, Zhang Y, Hadjipanayis G, Givord D and Nogués J 2003 *Nature* **423** 850
[13] Sort J, Nogués J, Amils X, Suriñach S, Muñoz J S and Baro M D 1999 *Appl. Phys. Lett.* **75** 3177
[14] Sort J, Suriñach S, Muñoz J S, Baró M D, Nogués J, Chouteau G, Skumryev V and Hadjipanayis G C 2002 *Phys. Rev.* B **65** 174420
[15] Nogués J, Sort J, Langlais V, Skumryev V, Surinach S, Munoz J S and Baro M D 2005 *Phys. Rep.* **422** 65
[16] Anhøj T A, Jacobsen C S and Mørup S 2004 *J. Appl. Phys.* **95** 3649
[17] Néel L 1949 *Ann. Geophys.* **5** 99
[18] Brown W F Jr 1963 *Phys. Rev.* **130** 167
[19] Mørup S and Hansen B R 2005 *Phys. Rev.* B **72** 024418
[20] Mørup S and Topsøe H 1976 *Appl. Phys.* **11** 63
[21] Mørup S 1983 *J. Magn. Magn. Mater.* **37** 39
[22] Martin D H 1967 *Magnetism in Solids* (Cambridge, MA: MIT Press)
[23] Néel L 1954 *J. Phys. Rad.* **15** 225
[24] Hansen M F, Bødker F, Mørup S, Lefmann K, Clausen K N and Lindgård P-A 1997 *Phys. Rev. Lett.* **79** 4910
[25] Lefmann K, Bødker F, Klausen S N, Hansen M F, Clausen K N, Lindgård P-A and Mørup S 2001 *Europhys. Lett.* **54** 526
[26] Trohidou K N 2005 *Surface Effects in Magnetic Nanoparticles* ed D Fiorani (New York: Springer) p 45
[27] Kodama R H and Berkowitz A E 2005 *Surface Effects in Magnetic Nanoparticles* ed D Fiorani (New York: Springer) p 189
[28] Coey J M D 1971 *Phys. Rev. Lett.* **27** 1140
[29] Morrish A H and Haneda K 1983 *J. Magn. Magn. Mater.* **35** 105
[30] Coey J M D 1987 *Can. J. Phys.* **65** 1210
[31] Mørup S 2003 *J. Magn. Magn. Mater.* **266** 110
[32] Bahl C R H, Hansen M F, Pedersen T, Saadi S, Nielsen K H, Lebech B and Mørup S 2006 *J. Phys.: Condens. Matter* **18** 4161
[33] Kodama R H, Makhlouf S A and Berkowitz A E 1997 *Phys. Rev. Lett.* **79** 1393
[34] Lindgård P-A 2003 *J. Magn. Magn. Mater.* **266** 88
[35] Bødker F, Hansen M F, Koch C B, Lefmann K and Mørup S 2000 *Phys. Rev.* B **61** 6826
[36] Klausen S N, Lindgård P-A, Lefmann K, Bødker F and Mørup S 2002 *Phys. Status Solidi* a **189** 1039
[37] Golosovsky I V, Mirebeau I, André G, Kurdyukov D A, Kumzerov Yu A and Vakhrushev S B 2001 *Phys. Rev. Lett.* **86** 5783
[38] Tsunoda Y, Nakano H and Matsuo S 1993 *J. Phys.: Condens. Matter* **5** L29
[39] Shinjo T, Kiyama M, Sugita N, Watanabe K and Takada T 1983 *J. Magn. Magn. Mater.* **35** 133
[40] Yamamoto A, Kiyama M and Shinjo T 1994 *Hyperfine Interact.* **92** 1311
[41] Yamamoto A, Honmyo T, Hosoito N, Kiyama M and Shinjo T 1993 *Nucl. Instrum. Methods* B **76** 202
[42] Trohidou K N, Zianni X and Blackman J A 1998 *J. Appl. Phys.* **84** 2795
[43] Bocquet S and Kennedy S J 1992 *J. Magn. Magn. Mater.* **109** 260
[44] Punnoose A, Magnone H, Seehra M S and Bonevich J 2001 *Phys. Rev.* B **64** 174420
[45] Zheng X G, Xu C N, Nishikubo N, Nishiyama K, Higemoto W, Moon W J, Tanaka E and Otabe E S 2005 *Phys. Rev.* B **72** 014464
[46] Bødker F and Mørup S 2000 *Europhys. Lett.* **52** 217
[47] Kündig W, Ando K J, Constabaris G and Lindquist R H 1966 *Phys. Rev.* **142** 327
[48] Schroeer D and Nininger R C 1967 *Phys. Rev. Lett.* **19** 632
[49] Klausen S N, Lefmann K, Lindgård P-A, Kuhn L T, Bahl C R H, Frandsen C, Mørup S, Roessli B, Cavadini N and Niedermayer C 2004 *Phys. Rev.* B **70** 214411
[50] Mørup S 1985 *Surf. Sci.* **156** 888
[51] Zysler R D, Fiorani D, Testa A M, Suber L, Agostinelli E and Godinho M 2003 *Phys. Rev.* B **68** 212408
[52] Guertin R P, Harrison N, Zhou Z X, McCall S and Drymiotis F 2007 *J. Magn. Magn. Mater.* **308** 97
[53] Gilles C, Bonville P, Wong K K W and Mann S 2000 *Eur. Phys. J.* B **17** 417
[54] Néel L 1961 *C.R. Acad. Sci. Paris* **252** 4075
[55] Richardson J T, Yiagas D I, Turk B, Forster K and Twigg M V 1991 *J. Appl. Phys.* **70** 6977
[56] Palkar V R, Ayyub P, Chattopadhyay S and Multani M 1996 *Phys. Rev.* B **53** 2167

[57] Pankhurst Q A 1991 *J. Magn. Magn. Mater.* **101** 291
[58] Harris J G E, Grimaldi J E, Awschalom D D, Chiolero A and Loss D 1999 *Phys. Rev.* B **60** 3453
[59] Kilcoyne S H and Cywinski R 1995 *J. Magn. Magn. Mater.* **140–144** 1466
[60] Makhlouf S A, Parker F T and Berkowitz A E 1997 *Phys. Rev.* B **55** R14717
[61] Seehra M S, Babu V S, Manivannan A and Lynn J W 2000 *Phys. Rev.* B **61** 3513
[62] Mørup S and Frandsen C 2004 *Phys. Rev. Lett.* **92** 217201
[63] Madsen D E and Mørup S 2006 *Phys. Rev.* B **74** 014405
[64] Vollath D, Szabó D V and Willis J O 1996 *Mater. Lett.* **29** 271
[65] Bañobre-López M, Vázquez-Vázquez C, Rivas J and López-Quintela M A 2003 *Nanotechnology* **14** 318
[66] Silva N J O, Amaral V S and Carlos L D 2005 *Phys. Rev.* B **71** 184408
[67] Madsen D E, Mørup S and Hansen M F 2006 *J. Magn. Magn. Mater.* **305** 95
[68] Hanson M, Johansson C and Mørup S 1993 *J. Phys.: Condens. Matter* **5** 725
[69] Respaud M 1999 *J. Appl. Phys.* **86** 556
[70] García-Palacios J L 2000 *Adv. Chem. Phys.* **112** 1
[71] Chantrell R W, Walmsley N, Gore J and Maylin M 2001 *Phys. Rev.* B **63** 024410
[72] Taketomi S and Shull R D 2003 *J. Magn. Magn. Mater.* **266** 207
[73] Makhlouf S A, Parker F T, Spada F E and Berkowitz A E 1997 *J. Appl. Phys.* **81** 5561
[74] Makhlouf S A 2002 *J. Magn. Magn. Mater.* **246** 184
[75] Lee G H, Huh S H, Jeong J W, Choi B J, Kim S H and Ri H-C 2002 *J. Am. Chem. Soc.* **124** 12094
[76] Kodama R H and Berkowitz A E 1999 *Phys. Rev.* B **59** 6321
[77] Hansen M F and Mørup S 1999 *J. Magn. Magn. Mater.* **203** 214
[78] Gittleman J I, Abeles B and Bozowski S 1974 *Phys. Rev.* B **9** 3891
[79] Jiang J Z and Mørup S 1997 *Nanostruct. Mater.* **9** 375
[80] Luis F, del Barco E, Hernández J M, Remiro E, Bartolome J and Tejada J 1999 *Phys. Rev.* B **59** 11837
[81] Allen P D, St Pierre T G, Chua-anusorn W, Ström V and Rao K V 2000 *Biochim. Biophys. Acta* **1500** 186
[82] Dickson D P E, Reid N M K, Hunt C, Williams H D, El-Hilo M and O'Grady K 1993 *J. Magn. Magn. Mater.* **125** 345
[83] Blume M and Tjon J A 1968 *Phys. Rev.* **165** 446
[84] Tronc E 1996 *Nuovo Cimento* D **18** 163
[85] Bødker F, Mørup S and Linderoth S 1994 *Phys. Rev. Lett.* **72** 282
[86] Mørup S and Ostenfeld C W 2001 *Hyperfine Interact.* **136** 125
[87] Mørup S, Clausen B S and Christensen P H 1987 *J. Magn. Magn. Mater.* **68** 160
[88] St Pierre T G, Jones D H and Dickson D P E 1987 *J. Magn. Magn. Mater.* **69** 276
[89] Morrish A H 1965 *The Physical Principles of Magnetism* (New York: Wiley)
[90] Yosida K 1996 *Theory of Magnetism* (Berlin: Springer)
[91] Mørup S 2007 *Europhys. Lett.* **77** 27003
[92] Hendriksen P V, Linderoth S and Lindgård P-A 1993 *Phys. Rev.* B **48** 7259
[93] Kittel C 1951 *Phys. Rev.* **82** 565
[94] Keffer F and Kittel C 1952 *Phys. Rev.* **85** 329
[95] Hansen M F, Bødker F, Mørup S, Lefmann K, Clausen K N and Lindgård P-A 2000 *J. Magn. Magn. Mater.* **221** 10
[96] Klausen S N, Lefmann K, Lindgård P-A, Clausen K N, Hansen M F, Bødker F, Mørup S and Telling M 2003 *J. Magn. Magn. Mater.* **266** 68
[97] Wangsness R K 1952 *Phys. Rev.* **86** 146
[98] Wangsness R K 1953 *Phys. Rev.* **91** 1085
[99] Kuhn L T, Lefmann K, Bahl C R H, Ancona S N, Lindgård P-A, Frandsen C, Madsen D E and Mørup S 2006 *Phys. Rev.* B **74** 184406
[100] Bahl C R H, Lefmann K, Kuhn L T, Lindgård P-A, Christensen N B, Melis H V and Mørup S 2006 *J. Phys.: Condens. Matter* **18** 11203
[101] Chikazumi S 1997 *Physics of Ferromagnetism* 2nd edn (Oxford: Clarendon)
[102] Chudnovsky E M and Günther L 1988 *Phys. Rev. Lett.* **60** 661
[103] Barbara B and Chudnovsky E M 1990 *Phys. Lett.* A **145** 205
[104] Chudnovsky E M 1995 *J. Magn. Magn. Mater.* **140–144** 1821
[105] Gider S, Awschalom D D, Douglas T, Mann S and Chaparala M 1995 *Science* **268** 77
[106] Barbara B, Wernsdorfer W, Sampaio L C, Park J G, Paulsen C, Novak M A, Ferré R, Mailly D, Sessoli R, Caneschi A, Hasselbach K, Benoit A and Thomas L 1995 *J. Magn. Magn. Mater.* **140–144** 1825
[107] Tejada J, Hernandez J M and del Barco E 1999 *J. Magn. Magn. Mater.* **196/197** 552
[108] Awschalom D D, Smyth J F, Grinstein G, DiVincento D P and Loss D 1992 *Phys. Rev. Lett.* **68** 3092

[109] Barbara B, Paulsen C, Sampaio L C, Uehara M, Fruchard F, Tholence J L, Marghand A, Tejada J and Linderoth S 1992 *Studies of Magnetic Properties of Small Particles* (New York: Elsevier Science) p 235
[110] St Pierre T G, Gorham N T, Allen P D, Costa-Krämer J L and Rao K V 2002 *Phys. Rev.* B **65** 024436
[111] Kodama R H, Berkowitz A E, McNiff E J and Foner S 1996 *Phys. Rev. Lett.* **77** 394
[112] Zhang J, Boyd C and Luo W 1996 *Phys. Rev. Lett.* **77** 390
[113] Djurberg C, Svedlindh P, Nordblad P, Hansen M F, Bødker F and Mørup S 1997 *Phys. Rev. Lett.* **79** 5154
[114] Hansen M F and Mørup S 1998 *J. Magn. Magn. Mater.* **184** 262
[115] Mamiya H, Nakatani I and Furubayashi T 1998 *Phys. Rev. Lett.* **80** 177
[116] Fiorani D, Dormann J L, Cherkaoui R, Tronc E, Lucari F, D'Orazio F, Spinu L, Nogues M, Garcia A and Testa A M 1999 *J. Magn. Magn. Mater.* **196/197** 143
[117] Hansen M F, Koch C B and Mørup S 2000 *Phys. Rev.* B **62** 1124
[118] Bødker F, Hansen M F, Koch C B and Mørup S 2000 *J. Magn. Magn. Mater.* **221** 32
[119] Frandsen C and Mørup S 2003 *J. Magn. Magn. Mater.* **266** 36
[120] Mørup S, Madsen M B, Franck J, Villadsen J and Koch C J W 1983 *J. Magn. Magn. Mater.* **40** 163
[121] Mørup S, Frandsen C, Bødker F, Klausen S N, Lefmann K, Lindgård P-A and Hansen M F 2002 *Hyperfine Interact.* **144/145** 347
[122] Frandsen C and Mørup S 2005 *Phys. Rev. Lett.* **94** 027202
[123] Frandsen C, Bahl C R H, Lebech B, Lefmann K, Kuhn L T, Keller L, Andersen N H, v Zimmermann M, Johnson E, Klausen S N and Mørup S 2005 *Phys. Rev.* B **72** 214406
[124] Tobler L, Kündig W and Savic I 1981 *Hyperfine Interact.* **10** 1017
[125] Frandsen C and Mørup S 2006 *J. Phys.: Condens. Matter* **18** 7079
[126] Xu M, Bahl C R H, Frandsen C and Mørup S 2004 *J. Colloid Interface Sci.* **279** 132
[127] Bocquet S, Pollard R J and Cashion J D 1992 *Phys. Rev.* B **46** 11657
[128] Banfield J F, Welch S A, Zhang H, Ebert T T and Penn R L 2000 *Science* **289** 751
[129] Burleson D J and Penn R L 2006 *Langmuir* **22** 402
[130] Penn R L, Erbs J J and Gulliver D M 2006 *J. Cryst. Growth* **293** 1
[131] Madsen D E, Hansen M F, Koch C B and Mørup S 2007 unpublished
[132] Seehra M S, Shim H, Dutta P and Manivannan A 2005 *J. Appl. Phys.* **97** 10J509
[133] Shim H, Manivannan A, Seehra M S, Reddy K M and Punoose A 2006 *J. Appl. Phys.* **99** 08Q503
[134] Bahl C R H and Mørup S 2006 *Nanotechnology* **17** 2835
[135] Frandsen C, Ostenfeld C W, Xu M, Jacobsen C S, Keller L, Lefmann K and Mørup S 2004 *Phys. Rev.* B **70** 134416
[136] Nogués J, Skumryev V, Sort J, Stoyanov S and Givord D 2006 *Phys. Rev. Lett.* **97** 157203